

Integration of mooring system design with floating wind farm layout optimization

L.L. Mascini

Image from [1]



Contents

Summary	iii
Acknowledgements	v
1 Introduction	1
1.1 Floating Offshore Wind Turbines	2
1.2 Wind farm layout optimisation	3
1.3 Mooring in Floating Wind	4
1.4 Design of mooring systems	5
1.5 Mooring Models	7
1.6 Optimisation Methods	7
1.7 Conclusion	8
1.8 Research Questions	8
2 Methodology	9
2.1 Floating Wind Farm Optimisation Problem	9
2.1.1 Combined wind farm optimisation problem	9
2.1.2 Separation of MSDOP and CWFOP	10
2.1.3 Elements within the FWFOP	11
2.1.4 Floating wind farm cable routing problem	12
2.2 Mooring System Design Optimisation Problem	13
2.3 Mooring System Response Modelling	15
2.4 Multi-Objective Mooring System Optimisation Methods	16
2.5 Single-Objective Mooring System Optimisation Method	17
2.6 Layout Optimisation Methods	18
2.7 Case Study	19
3 Results and Discussion	21
3.1 Mooring System Optimisation	21
3.1.1 Extreme Load Case Analysis	21
3.1.2 Multiple Objective Optimisation Progression	25
3.1.3 Final Results	33
3.2 Layout and Cable Routing Optimisation	34
3.2.1 Individual layouts	34
3.3 Optimization and Parameter Study	39
4 Conclusions and Recommendations	41

Summary

In this thesis, the integration of mooring design with the layout optimisation of floating offshore wind farms is investigated. The objective of the research is to devise a method to unite the two design processes and then evaluate the benefits of this approach. Further, it will be investigated how to model mooring systems in an optimisation problem, the stage of the wind farm design process at which mooring design can be integrated, the couplings between mooring design, turbine placement and cable routing that exist and must be used to arrive at an improved design, and to what extent the approach improves the design of the floating wind farm.

Floating wind farms are still in a developmental phase, but will be key to meet the energy goals of the future. However, floating wind farm design brings with it challenges that do not exist for bottom-fixed offshore wind farms. Chief among these challenges is the mooring system, which not only has a significant impact on the performance of the turbine, but also due to its potentially large footprint can force alterations to the layout of the inter-array electrical cables with which turbines are connected to each other and the substations. Particular focus in this regard is on catenary mooring systems, given they are common in existing demonstrator projects and have a large footprint.

In this thesis, mooring design will be performed through a multi-objective optimisation using the NSGA-II algorithm, where the objectives will be to minimise the anchor radius as well as the system cost, with constraints to ensure adequate performance in terms of handling motions and loads. The mooring system will be described by 5 design variables, the line length ratio, synthetic fraction, anchor radius, synthetic line diameter, and chain line diameter. The Pareto-optimal solutions from this optimization will then be used to optimize the layout and cable routing using an algorithm based on the work of Cazzaro and property of Vattenfall AB.

It is found that the Pareto-optimal designs have anchor radii ranging from 394 to 494 m, with system costs ranging from \$3.352 million to \$6.441 million. However, with current layout design methods, the turbine placement is done independently of mooring system parameters, and the cable routing is not affected by a change in mooring system. Thus, using the cheapest mooring system regardless of footprint is optimal on a farm level, using current layout design methods.

Acknowledgements

I would like to express my deepest gratitude to those who have supported and guided me throughout the course of my master's thesis. This journey would not have been possible without their invaluable assistance and encouragement.

First and foremost, I extend my sincere thanks to my university supervisors, Dr. Michiel Zaayer and Dr. Fabio Pierella. Dr. Zaayer, your expertise and insightful feedback were instrumental in shaping this research. Your patience and encouragement helped me to overcome numerous challenges, and your guidance was crucial in navigating through complex concepts. Dr. Pierella, your detailed reviews and constructive criticism pushed me to refine my work and achieve a higher standard of academic excellence. I am deeply grateful for your unwavering support and mentorship.

I would also like to thank Dr. Martin Kidd, my supervisor at Vattenfall. Dr. Kidd, your practical insights and professional guidance were essential in bridging the gap between theoretical research and real-world application. Your support in providing resources and facilitating access to data significantly enriched the quality of this study. Working under your supervision has been a rewarding experience, and I am grateful for the opportunity to learn from you.

Additionally, I wish to acknowledge the support of my colleagues at Vattenfall and my fellow students at the university. Your camaraderie and shared experiences made this journey more enjoyable and less daunting.

Furthermore, I extend my heartfelt appreciation to my family and friends. Your encouragement and belief in my abilities provided me with the strength and determination to persevere through the demanding phases of this research. Thank you for always being there for me.

Finally, I would like to thank my girlfriend, Freya, for encouraging me through difficult times, and always being willing to listen to my ramblings.

This thesis is a testament to the collective support and guidance I have received, and I am deeply thankful to all who contributed to its completion.

List of Figures

1.1	The components of a floating offshore wind turbine [14]	2
1.2	Comparison of different types of mooring: tension leg (A), taut (B), catenary (C), semi-taut (D)	4
1.3	Free body diagram of a segment of a mooring line [31]	6
2.1	Flowchart of the tiered constraints system	17
2.2	A proposed layout from the research of Cazzaro [16] for one area of instance C	18
2.3	Illustration of the mooring system configuration	20
3.1	Sankey Diagram of outcomes of designs for the load case analysis	22
3.2	Frequency of constraint violations for each load case	23
3.3	Side by side comparison of constraint violations for load cases with only a heading difference in sea conditions	23
3.4	Side by side comparison of constraint violations for load cases with only a wind heading difference	24
3.5	Frequency of violations of the constraints on horizontal excursion, force angle at anchor, and mooring line tension for load cases with 0° current and wave headings and a 60° wind heading	24
3.6	Progression of Anchor Radius	26
3.7	Proportion of solutions found that are feasible per generation	26
3.8	Quartiles of anchor radius per generation	27
3.9	Progression of Line Length Ratio	27
3.10	Progression of Line Length Ratio shown on reduced domain	28
3.11	Progression of Synthetic Fraction	28
3.12	Progression of the cumulative feasibility rate for different ranges of synthetic fraction	29
3.13	Progression of Chain Line Diameter	29
3.14	Progression of Synthetic Line Diameter	30
3.15	Objective functions of solutions after generation 0	30
3.16	Objective functions of solutions after generation 5	31
3.17	Objective functions of solutions after generation 25	31
3.18	Objective functions of solutions after generation 55	32
3.19	Progression of constraint violation rates per generation	32
3.20	Objective functions of solutions at the conclusion of the optimisation, with focus on the well-performing solutions	34
3.21	Placement of 30 turbines on wind farm instance B from the CWFOP with safety radius	35
3.22	Wind Rose for the Ten Noorden van de Waddeneilanden wind farm zone [55]	35
3.23	Optimal layout with the mooring system with an anchor radius of 394 m at a 0° offset with 30 turbines	36
3.24	Optimal layout with the mooring system with an anchor radius of 394 m at a 40° offset with 30 turbines	37
3.25	Optimal layout with the mooring system with an anchor radius of 394 m at a 80° offset with 30 turbines	37
3.26	Optimal layout with the mooring system with an anchor radius of 483 m at a 40° offset with 30 turbines	38
3.27	Optimal layout with the mooring system with an anchor radius of 494 m at a 40° offset with 30 turbines	38
3.28	Placement of 60 turbines on wind farm instance B from the CWFOP with safety radius	39
3.29	Final layout found in optimization for the mooring system with an anchor radius of 483 m at a 0° offset with 60 turbines	39
3.30	Relationship between the anchor radius of the mooring system with 40° offset and the NPV of a 30 turbine wind farm	40

3.31 Relationship between the costs of the mooring system with 40° offset and the NPV of a 30 turbine wind farm	40
3.32 Relationship between the anchor radius of the mooring system with all offsets and the inter-array cable costs of a 30 turbine wind farm	40

List of Tables

2.1	Outputs ϕ_i from RAFT simulations and analyses	14
2.2	Differences between frequency-domain FOWT models	15
2.3	Overview of constraints by tiers	17
2.4	Key parameters of the different line types relative to the nominal diameter d_c [mm] [31]	19
3.1	An overview of the load case parameters used for all possible load cases	21
3.2	Directional extreme wave conditions used for load cases	22
3.3	Parameters of the Critical Load Cases used in further simulations	25
3.4	Design variables and cost of solutions on the final Pareto front	34

1

Introduction

Climate change due to human greenhouse gas emissions continues to be a great threat to humanity, with the 1.1°C of warming since the pre-industrial era already causing increases in the frequency and severity of heatwaves, floods, droughts, and other extreme weather events [2]. Studies by the International Energy Agency conclude that in order to reach global net-zero by 2050 and avoid warming of more than 1.5°C, annual development of renewables such as wind energy must increase five-fold from levels seen from 2018 to 2020 [3].

While wind energy development has historically taken place overwhelmingly onshore, accounting for over 90% of current capacity [4], offshore development is an increasingly popular alternative, with capacity expected to triple between 2023 and 2028 and a growth rate 4 times as high as onshore wind [4]. To reach net-zero emissions by 2050 and limit warming to 1.5°C, this growth much still be further accelerated, as nearly 80 GW of offshore wind should be developed annually [3], up from less than 11 GW in 2023 [4].

The reason for moving development of wind energy assets offshore is threefold. Firstly, due to the lack of protrusions from the landscape and the water providing lower friction than land, wind nearer to the surface is a larger fraction of geostrophic wind than on land. This allows for more power production as there is simply more energy in the wind at low altitudes offshore than onshore. Secondly, turbines offshore are less restricted by noise and maximum height, and thus can operate with higher tip speeds and have larger rotor radii, improving efficiency. Finally, it can simply be easier to obtain approval for development of offshore wind turbines as it is less visible for people living nearby, as they can be placed much farther from where people live. However, offshore bottom-fixed wind still has some issues.

Bottom-fixed offshore wind is generally restricted to water depths of around 50 m or less, as jacket foundations become prohibitively expensive beyond this depth [5]. This restriction means that bottom-fixed offshore wind is applicable in only fairly shallow water. While the depth from which floating wind will be preferable to bottom-fixed is as of yet unknown as it is largely dependent on cost reductions in floating wind [6], it has been asserted that the minimum width for floating wind to be competitive will be between 50 and 150 m [5]. For certain countries, such as Scotland [7], offshore wind resources are dominated by a large fraction that is in depths at which bottom-fixed wind may not be preferred. The main advantage of floating wind is that the increase in costs with water depth is much less significant than for bottom-fixed wind [8], as mooring costs do not increase as dramatically as fixed foundation costs with depth. Due to the technology still being in its infancy, industrial scale applications for floating wind do not yet exist, as costs and uncertainty are still too high for businesses and governments alike to commit to large projects. Thus, it is necessary to further the understanding of floating offshore wind and decrease the costs associated with it. In order to do so, in this thesis, the relationship between the mooring systems of floating offshore wind turbines (FOWT) with wind farm layout optimisation will be investigated.

While FOWT mooring system costs increase less quickly with respect to water depth than the substructures of bottom-fixed offshore wind, mooring system cost variation due to other factors is one of the six design-related parameters that most strongly influence the LCOE of a floating offshore wind farm [9]. Furthermore, the inter-array cable (IAC) length is a design parameter that influences the LCOE to a similar degree [9], and as the

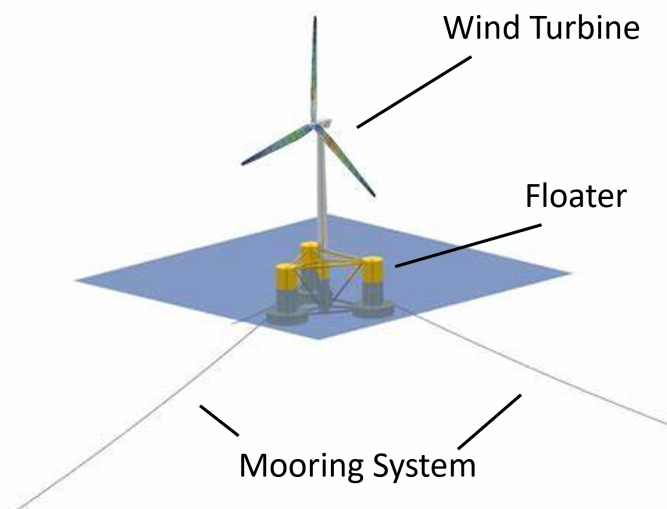


Figure 1.1: The components of a floating offshore wind turbine [14]

crossing and proximity of mooring lines and IACs is both restricted by regulations and significantly increases the cost of installation and maintenance, these costs are inherently interlinked. Thus, while many studies have been performed on how to optimise the mooring system itself, it is perhaps more important to optimise the mooring system in conjunction with the IACs. This will be the main objective of this thesis, an improved wind farm design through the integration of the mooring system optimisation with the optimisation of the IAC layout and wind farm layout.

1.1. Floating Offshore Wind Turbines

As opposed to bottom-fixed offshore wind turbines (BFWT), FOWTs are not connected to the seabed using a rigid structure, such as a monopile or jacket foundation. As shown in Figure 1.1, the wind turbine is supported by a floater which is then connected to the seabed with a system of mooring lines. The substructure uses a combination of buoyancy, mooring line tension, ballast weight, and hydrodynamic drag to absorb the forces imbued on the turbine and limit the motions and displacements of the turbine. The loads that the substructure must deal with can be split into the turbine loads, which are the aerodynamic and gravitational affecting the rotor and turbine tower, and the substructure loads, which are composed of the hydrodynamic and gravitational loads on the floater and mooring lines and the reaction forces and seabed friction on the lower part of the mooring lines and the anchor. One may notice that many of these loads can be dependent on each other, as, for example, the aerodynamic loads on the rotor will cause a motion that will alter the hydrodynamic and reaction forces on the substructure. The exact relationships between the different loads is dependent on the design of the turbine and substructure, and may be non-linear. This makes design of floating offshore wind turbines a complex process, and there are arguments to be made that many systems should be designed in an integrated or iterative manner, as performed in certain studies [10]. In this thesis, however, the focus will be on only the mooring system, with the usage of an existing turbine and floater. This will be the IEA 15 MW turbine [11] with the VolturnUS-S platform [12]. This platform is of the semi-submersible type, meaning that it is composed of a number of buoyant columns which are partly submerged (hence the name), and connected to each other and the turbine tower through pontoons. The VolturnUS-S has 3 buoyant columns at the corners of an equilateral triangle shape with a fourth centralised between them to support the turbine tower, which is modified from the standard IEA 15 MW design to better cope with the loading experienced in floating operation [12]. Semi-submersible floaters such as the one used in this thesis achieve stability through the horizontal spread of the buoyant elements [13]. They have particular advantages in construction, installation, and maintenance, as the draft is relatively low and the floater is quite stable immediately once constructed, and thus can be towed to the installation location in a finished state with the turbine already placed on top. The main disadvantages come due to its sensitivity to wave loads in particular, due to the width of the platform.

1.2. Wind farm layout optimisation

An overview and evaluation of the work done in wind farm layout optimisation is provided. Prior to 2012, most work was concerning onshore or bottom-fixed offshore wind farms, but many of the drivers and concerns carry over to the optimisation of floating wind farms. The problem is usually divided into two main considerations, being the objective to be achieved and the optimisation method [15]. While early studies used the Annual Energy Production (AEP), other studies found that this will often not result in the most economical solution, as the farm will be packed with the maximum feasible number of turbines, and the power production per turbine may be quite low. Thus, different objective functions that attempted to balance the financial investment required and the energy produced, such as the LCOE, Net Present Value (NPV), or the profit of the project. The diversity in exact definitions and what is included in the costs obfuscates the performance of each optimisation algorithm. However, the costs of as many components as possible should be considered, and the LCOE and NPV can be evaluated more quickly in a relative manner, thus not requiring the recalculation of the whole objective function at each point but only the delta to the previous iteration.

Furthermore, common methods of optimisation are established, which include gradient methods, genetic algorithms, viral algorithms, particle swarm algorithms, and greedy heuristic algorithms [15]. Gradient methods evaluate the derivatives of the objective function about possible solutions, and thus converge generally to local maxima or minima. Furthermore, in an optimisation problem with many parameters to optimise, as in the case of the optimisation of an industrial-scale wind farm layout, the calculation of derivatives can be computationally expensive. Thus, generally they are only used as a refinement step after the usage of another algorithm. Genetic, viral, and particle swarm algorithms all randomly generate a population of possible solutions. Then, they replace the poorly performing solutions by solutions which are more similar to the well performing solutions. Notably, the particle swarm algorithms can only optimise the location of a set number of turbines, rather than optimising both the number and location of turbines. However, they do not restrict the turbine locations to a pre-determined grid, as the genetic algorithm does. Finally, the greedy heuristic algorithms also start with a randomly initialisation, but here only one layout is used. New layouts are generated by making small changes to the existing layout, being to either add, remove, or move a turbine, and then replacing the old layout with the new one only if the new layout improves on the old one. Like the gradient methods, this is more prone to finding local rather than global optima.

One important study in offshore wind farm layout optimisation is the work of Cazzaro [16], which was an investigation into a unified design of the wind farm layout and intra-array cable routing for bottom-fixed offshore wind. The design of a bottom-fixed offshore wind farm consists of two optimization problems, the wind farm layout optimization problem and the wind farm cable routing problem. In the wind farm layout optimization problem (WFLOP), the placement of turbines within a defined area is performed in such a way that wake losses and foundation costs are minimised. In the wind farm cable routing problem (WFCRP), however, the connections between turbines with power cables are selected in order to minimise costs and avoid crossings and obstacles. The reason for unifying these two optimization problems is that the most ideal scenario for the WFLOP is to have the turbines spread out as much as possible, while the WFCRP has a better result with turbines which are closer together. As both problems are NP-hard, meaning they are at least as hard as the hardest nondeterministic polynomial time (NP) problems, a heuristic variable neighbourhood search (VNS) method is used to find solutions, with results evaluated using NPV, in order to correctly balance the different objectives. This method allowed for significant improvements in wind farm design, with better utilization of space (as it might not always be beneficial to use the entire space given in a tender) as well as improvements of up to 8 million euros in the NPV of wind farms.

Further research has been done into the layout optimisation of floating wind farms. In one study, mooring systems were designed to passively allow movement that would aid energy production by passively relocating turbines to minimise wake losses [17]. It was concluded from the initial study that relocations up to 1.2 times the rotor diameter were possible, by using the mooring line headings to direct the maximum motions and that lower stiffness systems were capable of more motion, with anchor radius not having a significant effect as all systems investigated were catenary mooring systems. A floating wind farm was designed using these conclusions for maximum AEP given a baseline layout [18]. This was done by creating a mooring systems database, of many feasible mooring designs and then allocating a mooring design from the database to each turbine in an optimisation loop. An increase in AEP of 1.3% was found from this approach on a farm with 19 IEA 15MW reference turbines. In a sensitivity analysis of the previous result, it was found that on smaller wind farms the relative energy gains are larger than for a larger wind farm, with the improvements at 10 m/s

wind speeds being approximately 30% less for a wind farm with about twice as many turbines, but that this difference becomes smaller when the wind rose becomes less mono-directional [19]. The benefits are further halved when a dynamic wake model is used in the analysis rather than steady state, but that ultimate loads on mooring systems using this design are less than for a conventional design [20].

The combination of active turbine repositioning with yaw misalignment for wind farm optimisation was also investigated [21]. This would involve position mooring systems where winches are used to adjust mooring line lengths during operation [22]. Yaw misalignment requires only to adjust the controller optimal yaw angle, and thus requires no extra sensors or actuators, making it an attractive option to improve a floating wind farm as it provides significant power benefits, particularly when the free stream wind speed is just above the rated wind speed, such that leading turbines can yaw without power losses while increasing power for trailing turbines [21]. In these conditions, yaw misalignment can increase power by 11% in a wind farm of 16 turbines, with about 3% increases in power in sub-rated conditions. Active turbine repositioning can increase wind farm power by up 5-8% depending on the free stream wind speed for a movable range of 0.5 rotor diameters, with benefits increasing hyperbolically with movable range. Increasing the movable range beyond 2 rotor diameters provides limited benefits, as at this point wake losses only account for 3% of the total power, and the installation positions do not significantly affect the energy production [22]. The combination of both turbine repositioning and yaw misalignment does not offer significant benefits over only turbine repositioning, while the benefits over only yaw misalignment are inconsistent [21].

1.3. Mooring in Floating Wind

Mooring design is a long-studied field, as the technologies used for wind turbine mooring are similar to mooring in the oil and gas industry [23]. However, due to the differences in loading conditions and requirements, that oil-and-gas derived mooring systems may be too conservative and can be optimised further. Particular differences include the fact that the mooring systems for floating wind do not require redundancy, as the environmental effects of a mooring failure on a FOWT are much less severe than for an oil or gas installation, and that movement and offset requirements are defined mostly by turbine fatigue and electrical cable flexibility, rather than restrictions for the safety of crew on oil and gas installations which largely drive these requirements. This is exemplified by IEC standard 61400-3-2 [24] which covers floating offshore wind but simply cites ISO 19901-7 [25], an oil and natural gas standard, when discussing mooring systems.

There are currently no industrial-scale floating wind farms in existence, but a number of demonstrator projects have been commissioned or are planned [26]. These projects have water depths ranging from 29 to 300 m, with up to 11 turbines in a single project which range up to 10 MW in rated power. Notably, all but 2 of the demonstrator projects use a catenary mooring system, with a combination of mostly semi-submersible and spar buoy floaters used. An example of the main types of mooring systems used in floating wind is shown in Figure 1.2.

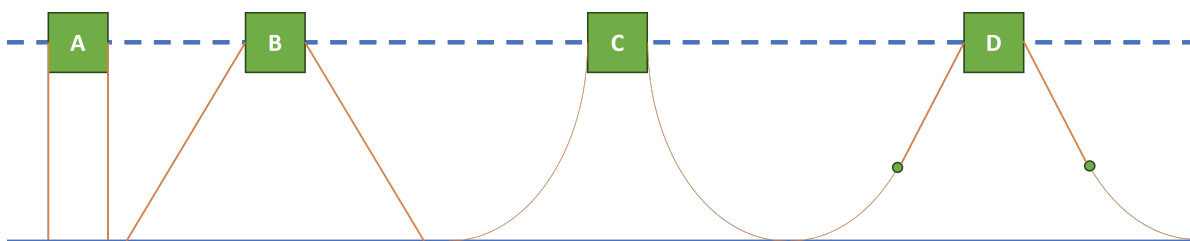


Figure 1.2: Comparison of different types of mooring: tension leg (A), taut (B), catenary (C), semi-taut (D)

Catenary mooring is a type of mooring system which uses suspended mooring lines whose gravity provides the vertical restoring force such that the ends of the lines lie on the seabed and loads the anchor only in horizontal direction. It is commonly used at water depths less than 500 m, because of its simplicity and reliability. However, it has the downside of having a large footprint, especially at larger water depths.

At larger water depths, it may be beneficial to instead use taut mooring. In taut mooring, the mooring lines are always taut in tension, at an angle of 30-45 degrees from the seabed. This requires anchors which can provide vertical as well as horizontal restoring forces. Generally, light and strong synthetic materials such as

polyester and nylon are used for taut moorings, rather than the chains typically used for catenary moorings [26], [27]. Taut moorings provide a larger restoring force [26], reducing the movement of the floater, while synthetic lines are cheaper in cost per meter [27], as well as being lighter, making them easier to transport and reducing the loads on the floater [26]. Due to the direct path to the seabed, the lengths and footprint of taut moorings are less than catenary moorings, however, they are more complex, making them more expensive to manufacture and install, as well as being more prone to fatigue failure due to the high alternating loads in the mooring lines.

There are two more types of mooring which are less widely used. The first is a compromise between catenary and taut mooring, which is known as semi-taut mooring and is used in the only 2 demonstrator projects not to use catenary moorings [26]. Semi-taut mooring uses a combination of a taut mooring line between the floater and an underwater buoy, with catenary moorings connecting the buoy to the anchor. While Yang et al. [26] assert that it is financially competitive while having performance similar to a taut mooring system, a design analysed by Fulton et al. [27] was significantly more expensive at a water depth of 132 m than taut or catenary moorings, while also possessing by far the largest footprint of the 4 designs proposed. In this study, the catenary and taut moorings were found to be very similar in total costs, which is surprising, as this would usually be too shallow for taut mooring to be effective [23].

One more type of mooring should be covered, which is associated with a particular floater concept, that being the tethered mooring used for a tension leg platform (TLP). The tethers are a series of steel tubes which are attached between the float and the anchors in a purely vertical direction [26]. They provide very high stiffness and an almost negligible footprint, however the floater in a TLP is not stable on its own, and thus the tethers have to provide this. Thus, if a tether breaks, there is a high likelihood that the FOWT will capsize. Due to their importance for averting the loss of a turbine, the production is extremely precise, while the installation is highly challenging, meaning the costs are high. Also, due to the very high stiffness of the tethers and that they are pre-tensioned, the natural frequencies in the heave direction will be extremely high, which can cause resonance issues induced by waves [28]. As floating wind mooring systems do not necessarily require inbuilt redundancy, these drawbacks make the TLP less financially competitive than other options [26]. The optimisation of TLP tethers will also not have any interactions with the cable routing and turbine placement as the tethers are directly vertical. For these reasons, TLPs and their mooring systems will not be considered in this thesis.

The different types of mooring also require different types of anchors due to the different loading conditions imposed on the anchors. Catenary and semi-taut mooring systems impose almost no vertical loads on the anchors [27], and thus drag embedded anchors can be used, while for taut moorings, other anchor types have to be used. Drag embedded anchors are very easy to install and manufacture, are relatively small, and can be used in all sediments [27], [29], thus they are very commonly used. However, one main drawback is that they cannot be placed as precisely as other anchor types, thus they may not be as advantageous in a dense wind farm layout [27]. Many other anchoring systems are attested to in the literature, however, as in this thesis the focus will be on catenary systems, and the anchors will not be modeled in significant depth, a further discussion of these anchors is not relevant.

1.4. Design of mooring systems

In general, mooring design is an iterative process, whereby an initial standard mooring design is evaluated over several load cases, upon which changes are made to the design with the aim of reducing the cost of the mooring system or meeting unmet requirements [30]. Typically, the type of mooring system, whether catenary, semi-taut, or taut, is selected a priori, and then the necessary stiffnesses and weights of components are iteratively designed, after which the off-the-shelf components that meet the requirements can be selected. Once the stiffnesses and weights are known, the anchor is then sized based on the forces calculated in the previous step and the seabed conditions.

The stiffnesses and weights of the main components of a mooring line are designed based on the loading and displacements experienced by the system over a number of load cases. The loading and displacements on a segment of a mooring line are shown in Figure 1.3. Here, the tension T , stiffness of the line AE , and hydrodynamic forces in the tangential and normal direction F_ϕ and F_ψ over a segment of length dl are used. Transverse bending and torsion are not included, as the large radius of curvature in mooring lines makes these factors negligible [31]. From this diagram, the equations shown in Equation 1.1 can be constructed [31].

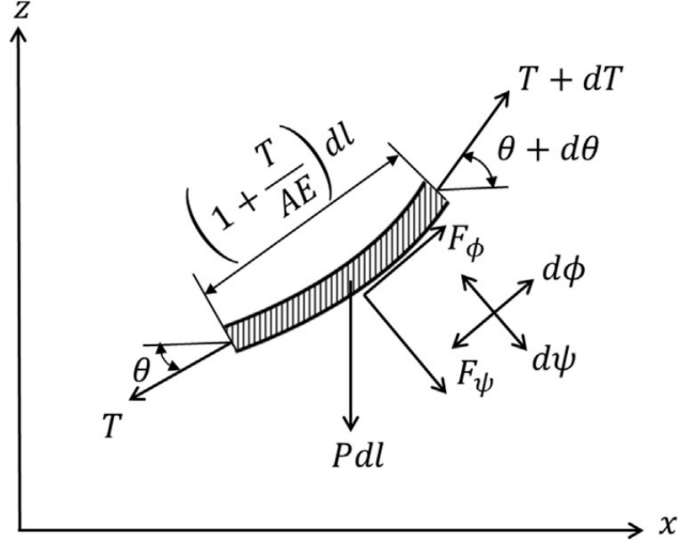


Figure 1.3: Free body diagram of a segment of a mooring line [31]

$$m \frac{d^2 \phi(l)}{dt^2} = dT - P \sin \theta dl + F_\phi \left(1 + \frac{T}{AE}\right) dl \quad (1.1.1)$$

$$m \frac{d^2 \psi(l)}{dt^2} = T d\theta - P \cos \theta dl - F_\psi \left(1 + \frac{T}{AE}\right) dl \quad (1.1.2)$$

$$dx = \left(1 + \frac{T}{AE}\right) \cos \theta dl \quad (1.1.3)$$

$$dz = \left(1 + \frac{T}{AE}\right) \sin \theta dl \quad (1.1.4)$$

$$d\phi = dz \cos \theta - dx \sin \theta \quad (1.1.5)$$

$$d\psi = dx \cos \theta + dz \sin \theta \quad (1.1.6)$$

These equations can be solved in a variety of ways, depending on the application. One such solution is known as the catenary equation, which describes the shape of a catenary mooring line under a static loading with inelastic components [31]. However, more commonly, these equations are solved numerically, using some form of finite element analysis. Certain such models are described in section 1.5. The hydrodynamic forces on the mooring line are usually defined using some solution of the Navier-Stokes equations, particularly the Morison equation.

The Morison equation describes the force exerted by waves on a cylindrical structure as the combination of a drag force and an a "virtual mass force" **Morison**. The main equation is formulated as shown in Equation 1.2 **Sarpkaya**, but many variations that take into account the movement of the structure, currents, and other factors also exist [31].

$$dF = \left[C_D \rho \frac{D}{2} u^2 + C_M \rho \pi \frac{D^2}{4} \frac{\partial u}{\partial t} \right] dz \quad (1.2)$$

Another avenue of research is the concept of shared mooring and shared anchors. While multiple concepts exist, the general idea is to reduce the number of necessary components by using each line or anchor to moor multiple FOWTs. This introduces a number of other factors to consider for mooring design in a farm context, such as which turbines can be moored together to still allow for a feasible IAC routing and couplings between the motions of different turbines, and thus is considered outside the scope of this thesis.

1.5. Mooring Models

MoorDyn, developed by Hall and Goupee [32], is one of the most prevalent mooring models used in literature. It uses a discretised model of the mooring cables into nodes and the segments between them. The mass is lumped at the nodes, while internal tension and damping is calculated in each segment. Hydrodynamic drag is modelled using the Morison equation, while a linear spring-damper is used to model the vertical reaction forces from the seabed to interaction with the cables. In further development [33], the force of friction between the cable and seabed was also added. Non-linear stiffness behaviour is also supported [34]. For full-system simulations, it is usually combined with OpenFAST.

QuLAF is a frequency-domain, linearised model for the analysis of loads on floating offshore wind turbines by Pegalajar-Jurado et al. [35]. For mooring, this model takes some results of simulations in MoorDyn, before simulating the response of the wind turbine and floater. QuLAF requires an initial simulation at each wind speed to find the equilibrium position, as well as two simulations per degree of freedom (surge, heave, and pitch) to find the stiffness. Thus, it requires 7 time-domain simulations, however, these are fairly simple and short time-domain simulations. QuLAF, furthermore, pre-computes hydrodynamic and aerodynamic loads from other software, being WAMIT and OpenFAST, which in this analysis would only have to be done once during the process of optimising the mooring system, with predictions for natural frequencies, responses, and loads being able to be calculated for multiple environmental conditions. In comparison to a full time-domain simulation in a state-of-the-art model [36] and based on the tools mentioned previously, it has no error in surge, errors of less than 1.5% in heave and pitch, and less than 10% in the natural frequency of the tower. The biggest limitation to QuLAF, is the under-prediction of nacelle accelerations due to “an over-prediction of the aerodynamic damping on the tower mode” [37] and a non-conservative estimation of the loads due to wave excitation, but the model is nonetheless accurate enough for use in a preliminary design stage, and thus is suitable for use in this thesis. QuLAF can be used for the optimisation of a mooring system [38], [39].

QuLAF could also be combined with an analytical solution for the mooring stiffness matrix [40]. Here, an analytical solution for the mooring stiffness from the vertical and horizontal tension on the fairlead as well as design parameters such as unstretched cable length, weight, and extensional stiffness. This calculation could thus replace 6 of the 7 MoorDyn simulations necessary in the standard QuLAF procedure without loss of generality or accuracy. Such an approach is also used by Dou et al. [39]. However, QuLAF is not currently a public software, and while the theoretical basis is public, the implementation of such a model is outside the scope of this thesis.

A final set of models that is worth mentioning is RAFT and MoorPy. RAFT is a frequency-domain model for floating wind turbine design, developed by Hall et al. [41]. MoorPy, the mooring component of RAFT, is a quasi-static model specifically designed to better support mooring design, rather than analysis of an existing design [42]. RAFT was developed to allow integrated design and optimisation of the turbine, floater, controller, and mooring. The agreement between RAFT and OpenFAST is good, with errors for FOWT motions generally under 10% [41]. However, it should be noted that the mooring tension response tends to have larger errors due to the lack of dynamic effects in MoorPy. An upcoming paper asserts that the differences in steady-state displacements between MoorPy and OpenFAST are negligible [20], but this paper is yet to be reviewed for publication. It should be noted however, that this is the latest in a series of publications by Mahfouz et al. [17]–[19], all of which have used the MoorPy model.

1.6. Optimisation Methods

Two main methods for optimisation are attested to in literature. The first is described by [43] and uses a genetic algorithm. Specifically, it uses NSGA-II, a genetic algorithm developed by [44] which, rather than optimising for a single objective function and thus finding one optimal solution, optimises for multiple (usually 2) objective functions, and finds sets of solutions which are non-dominated, meaning there is no other solution which has better performance in all objective functions. Thus, unless there is one solution which is the optimal solution for both objective functions, it will realise a Pareto front. In the research by [43], the optimisation algorithm has two objective functions, one to minimise the mooring cost, and the other to minimise the fatigue damage. However, one could also imagine that the fatigue damage could be a constraint instead and the mooring radius should instead be minimised, which is how this algorithm would be applied to this thesis. This is exactly what is done by [45] and [46], where this is coupled with a tiered evaluation

of constraints. This means that constraints are calculated in groups based on computational expense, with less computationally expensive constraints evaluated first, and ending the evaluation of a design if there are constraints that are not fulfilled in a group before proceeding to the next group of constraints. This is done because some of the mooring analysis in this method is performed using MoorDyn, which, due to being a time-domain simulation, is much more computationally expensive than frequency-domain methods. However, [45] maintain that these time-domain simulations are necessary as frequency-domain models can have significant non-conservative errors when predicting mooring line tension.

The second method, used by [39], is a sequential quadratic programming (SQP) method, with the derivatives of the frequency-domain response and the eigenvalues with respect to the design variables being calculated analytically a priori. SQP methods are iterative methods which model the problem as quadratic at each step to make a new approximation [47]. Thus, it can be seen as an extension to Newton's Method. However, crucially, this method is a single-objective optimisation method, which would require multiple separate optimisations be run to get a diverse range of mooring systems with different mooring radii. Another drawback of the previous method is that it is a continuous optimisation method, whereas in reality some of the design variables may have only a finite number of discrete options. [38] build on the work of [39] by adding two further optimisation methods to essentially post-process the solution of the first optimisation problem. The second optimisation problem solved is a mixed-integer linear programming (MILP) problem which is applied to the initial solution to map it onto a catalogue of available designs. Then, as it is possible that the mapping onto the catalogue may not have found the most optimal solution in the catalogue, a heuristic is applied locally to test all adjacent solutions to the current solution in the design space and updating the design if an improvement is found. This combination of methods allows the elimination of engineering judgement choosing a suboptimal solution once the initial continuous solution is found.

1.7. Conclusion

As shown, the design and optimisation for mooring systems in floating wind energy has seen significant research with wide-reaching topics, from suitability of certain types of mooring systems and anchors, to the optimisation of wind farm layouts and mooring systems for a particular turbine/floater and certain environmental conditions. However, there is no established literature investigating the optimisation of mooring systems within a larger, arbitrarily dense wind farm, and in particular the interaction between mooring lines and IACs. This is the gap that this thesis will aim to fill, supplementing the understanding of mooring system design for FOWTs by investigating a more practical context where the mooring system must interact with other systems in an industrial-scale floating wind farm. This thesis will be done by expanding on the work of Cazzaro [16], to bring the tool developed into the floating domain by adding mooring design optimisation and working on the integration of it into the layout optimisation.

1.8. Research Questions

Thus, the main research question driving this thesis is as follows. How can mooring systems design be integrated into the wind farm layout optimisation process and what benefits can this bring? Due to the complexity of answering this question directly, it can be helpful to break the thesis into multiple sub-questions, the answers to which will together provide an answer to the main research question. These sub-questions are listed below.

- Which mooring models are best suited for use in an optimisation context?
- At what stage of the wind farm layout optimisation process can mooring system design be best implemented?
- What couplings between mooring design, turbine layout, and cable routing are necessary to produce an improved wind farm design?
- To what extent does the integrated wind farm layout and mooring optimisation improve the design of the wind farm?

2

Methodology

2.1. Floating Wind Farm Optimisation Problem

2.1.1. Combined wind farm optimisation problem

The CWFOP is formulated by Cazzaro [16] as in Equation 2.1. Where \mathcal{N} is the set of available turbine positions on which to build T turbines. The binary variable x_i denotes whether a turbine is built in position i or not, while y_{ij}^k is a binary variable denoting whether the turbines at positions i and j are connected by an electrical cable of capacity k from the set of available cable types \mathcal{K} . The optimisation attempts to maximise the combination of the discounted energy revenue LER , the foundation cost FOU , and the cable cost CBL , as shown in Equation 2.1.1. This is done using an aggregated discounted energy price constant EP , the wake matrix with the power production of turbines in free stream P_{ii} and the power losses of turbine j due to the wake of turbine i in P_{ij} , the foundation costs per location F_i , the distance between two turbines d_{ij} , the length of a cable between two turbines b_{ij} , and the cost per unit length of a cable of a certain type c^k . Further constraints are used to incorporate a minimum distance requirement m , the power flows in array cables f_{ij} , the location of the substation s with $\mathcal{N}_s := \mathcal{N} \cup \{s\}$, the number of cables connected to the substation W , and the set of cables that cross each other \mathcal{C} .

$$\max \quad LER(x) - FOU(x) - CBL(x, y) \quad (2.1.1)$$

$$= EP \sum_{i \in \mathcal{N}} \sum_{j \in \mathcal{N}} P_{ij} x_i x_j - \sum_{i \in \mathcal{N}} F_i x_i - \sum_{i \in \mathcal{N}_s} \sum_{j \in \mathcal{N}_s} \sum_{k \in \mathcal{K}} b_{ij} c^k y_{ij}^k \quad (2.1.2)$$

$$\text{s.t.} \quad \sum_{i \in \mathcal{N}} x_i = T \quad (2.1.3)$$

$$x_i + x_j \leq 1 \quad \forall i, j \in \mathcal{N}, d_{ij} \leq m \quad (2.1.4)$$

$$x_i \in \{0, 1\} \quad \forall i \in \mathcal{N} \quad (2.1.5)$$

$$\sum_{k \in \mathcal{K}} y_{ij}^k \leq x_i \quad \forall i, j \in \mathcal{N}_s \quad (2.1.6)$$

$$\sum_{k \in \mathcal{K}} y_{ij}^k \leq x_j \quad \forall i, j \in \mathcal{N}_s \quad (2.1.7)$$

$$\sum_{j \in \mathcal{N}_s} \sum_{k \in \mathcal{K}} y_{ij}^k = x_i \quad \forall i \in \mathcal{N} \quad (2.1.8)$$

$$\sum_{j \in \mathcal{N}_s} \sum_{k \in \mathcal{K}} y_{sj}^k = 0 \quad (2.1.9)$$

$$f_{ij} \leq \sum_{k \in \mathcal{K}} k y_{ij}^k \quad \forall i, j \in \mathcal{N}_s \quad (2.1.10)$$

$$\sum_{j \in \mathcal{N}_s} f_{ij} = \sum_{l \in \mathcal{N}_s} f_{li} + x_i \quad \forall i \in \mathcal{N} \quad (2.1.11)$$

$$\sum_{i \in \mathcal{N}} f_{is} = |\mathcal{N}| \quad (2.1.12)$$

$$\sum_{i \in \mathcal{N}} \sum_{k \in \mathcal{K}} y_{is}^k = W \quad (2.1.13)$$

$$\sum_{i \in \mathcal{N}} \sum_{k \in \mathcal{K}} y_{ij}^k \leq x_j \quad \forall j \in \mathcal{N} \quad (2.1.14)$$

$$\sum_{k \in \mathcal{K}} y_{ij}^k + \sum_{k \in \mathcal{K}} y_{mn}^k \leq 1 \quad \forall (\{i, j\}, \{m, n\}) \in \mathcal{C} \quad (2.1.15)$$

$$y_{ij}^k \in \{0, 1\} \quad \forall i, j \in \mathcal{N}_s, k \in \mathcal{K} \quad (2.1.16)$$

$$f_{ij} \geq 0 \quad \forall i, j \in \mathcal{N}_s \quad (2.1.17)$$

$$0 \leq f_{ij} \leq \left\lceil \frac{|\mathcal{N}|}{W} \right\rceil \quad \forall i, j \in \mathcal{N}_s \quad (2.1.18)$$

$$\left\lceil \frac{|\mathcal{N}|}{W} \right\rceil \sum_{k \in \mathcal{K}} y_{ij}^k \leq f_{ij} \quad \forall i, j \in \mathcal{N}_s \quad (2.1.19)$$

2.1.2. Separation of MSDOP and CWFOP

To incorporate the mooring system into this optimisation, it must first be decided in what manner this incorporation should take place. From the perspective of the overall optimisation, the mooring system can be summarised by 2 key characteristics, being the anchor locations and the cost of the mooring system. Furthermore, it is not advantageous from a manufacturing and installation perspective to have a bespoke mooring system for each turbine, as it will not be possible to take advantage of economies of scale in this case. While it is necessary to design the mooring system to a certain level to be able to assess the feasibility as well as the cost and anchor locations, this level of detail is not necessary in the optimisation of the wind farm layout. Thus, the MSDOP, which is detailed in section 2.2, will not be included in the overall optimisation, but will, similarly to the wake matrix or the set of available cables, be performed as a pre-processing step to the main optimisation, resulting in a set of mooring systems with each a different anchor radius and mooring system cost.

It is important to note however, that this does not necessarily mean that the anchor locations are set given a certain turbine location. While misalignment of loads with the mooring system would require an extra safety factor, accounting for this would mean that the mooring system could be rotated about the turbine, potentially improving the cable routing solution. Both mooring systems designed to be able to rotate and

mooring systems with fixed orientations will be tested in this thesis, but to avoid a loss of generality, the optimisation problem will be formulated assuming rotation of mooring systems is possible within the wind farm design optimisation.

It is also important to realise, with regard to the implementation of the mooring systems in the way presented here, that in order to take advantage of economies of scale most effectively, the mooring systems must be the same for each turbine. This thus also necessitate a mooring design which must be feasible for a range of water depths and soil conditions. However, if the water depths of the chosen site are varied, this might necessitate a mooring design which is significantly more costly than optimal for most potential turbine locations in the site. Thus, it is easy to imagine a scenario where in fact it would be more cost-effective to instead have multiple sets of mooring designs for different ranges of water depths present in the site. In this thesis, it will initially be assumed that the range of water depths is narrow enough that this is not the case, but this could be investigated in an extension. Nevertheless, in the formulation of the optimisation problem here, it will be assumed that every turbine will use the same mooring system.

2.1.3. Elements within the FWFOP

It is possible and beneficial to combine the wind farm layout optimisation problem (WFLOP) and the wind farm cable routing problem (WFCRP) into the CWFOP [16]. However, the CWFOP in the form shown in subsection 2.1.1 was devised for bottom-fixed offshore wind farms, and while it is at first glance not necessary to make major changes to allow for the addition of the mooring system, this is not in actuality so simple. This is because of the determination of the length of a cable between two turbines. In the CWFOP for bottom-fixed offshore wind farms, it is sufficient to incorporate any environmental obstacles on the seabed where IACs may not pass through by pre-processing the matrix b_{ij} and computing the lengths of alternate paths whenever the straight path would pass through an obstacle. However, in a floating wind farm the anchors of mooring lines also function as obstacles, with the separation of IACs and anchors having to be at least 100 m [25], and mooring lines and IACs are also not allowed to cross. Thus, the length of cables between turbines is no longer feasible to precompute due to the number of options of where the mooring systems might be located. Instead, the cable paths must be computed using an algorithm, such as the one proposed by Janus [48], for each change in the mooring system.

Due to the increased computation necessary for this calculation, in addition to the addition of a further system to include in the optimisation, it may be too computationally expensive, as well as very complex, to solve a floating wind farm optimisation problem including the WFLOP, WFCRP, and the mooring system simultaneously. Instead, it is proposed that the CWFOP [16] will be used to establish the position of the turbines and provide an initial solution for the cable routing. Then, with a fixed turbine layout, the mooring system and cable routing will be jointly optimised in the floating wind farm cable routing problem (FWFCRP), which is illustrated in subsection 2.1.4. The FWFOP can thus be described entirely by the sequential combination of the CWFOP and the FWFCRP.

2.1.4. Floating wind farm cable routing problem

By extension from the WFCRP as formulated by Cazzaro [16], the FWFCRP (floating wind farm cable routing problem) can be formulated as follows:

$$\min \quad CBL(y) + MOO(z) \quad (2.2.1)$$

$$= \sum_{i \in \mathcal{T}_s} \sum_{j \in \mathcal{T}_s} \sum_{k \in \mathcal{K}} b_{ij}(z_i^m) c^k y_{ij}^k + \sum_{i \in \mathcal{T}_s} \sum_{m \in \mathcal{M}} c^m z_i^m \quad (2.2.2)$$

$$s.t. \quad \sum_{k \in \mathcal{K}} y_{ij}^k \leq 1 \quad \forall i, j \in \mathcal{T}_s \quad (2.2.3)$$

$$\sum_{j \in \mathcal{T}_s} \sum_{k \in \mathcal{K}} y_{ij}^k = 1 \quad \forall i \in \mathcal{T} \quad (2.2.4)$$

$$\sum_{j \in \mathcal{T}_s} \sum_{k \in \mathcal{K}} y_{sj}^k = 0 \quad (2.2.5)$$

$$f_{ij} \leq \sum_{k \in \mathcal{K}} k y_{ij}^k \quad \forall i, j \in \mathcal{T}_s \quad (2.2.6)$$

$$\sum_{j \in \mathcal{T}_s} f_{ij} = \sum_{l \in \mathcal{T}_s} f_{li} + 1 \quad \forall i \in \mathcal{T} \quad (2.2.7)$$

$$\sum_{i \in \mathcal{T}} f_{is} = |\mathcal{T}| \quad (2.2.8)$$

$$\sum_{i \in \mathcal{T}} \sum_{k \in \mathcal{K}} y_{is}^k = W \quad (2.2.9)$$

$$\sum_{i \in \mathcal{T}} \sum_{k \in \mathcal{K}} y_{ij}^k \leq 1 \quad \forall j \in \mathcal{T} \quad (2.2.10)$$

$$\sum_{k \in \mathcal{K}} y_{ij}^k + \sum_{k \in \mathcal{K}} y_{np}^k \leq 1 \quad \forall (\{i, j\}, \{n, p\}) \in \mathcal{C}_{kk} \quad (2.2.11)$$

$$y_{ij}^k \in \{0, 1\} \quad \forall i, j \in \mathcal{T}_s, k \in \mathcal{K} \quad (2.2.12)$$

$$f_{ij} \geq 0 \quad \forall i, j \in \mathcal{T}_s \quad (2.2.13)$$

$$0 \leq f_{ij} \leq \left\lceil \frac{|\mathcal{T}|}{W} \right\rceil \quad \forall i, j \in \mathcal{T}_s \quad (2.2.14)$$

$$\left\lceil \frac{|\mathcal{T}|}{W} \right\rceil \sum_{k \in \mathcal{K}} y_{ij}^k \leq f_{ij} \quad \forall i, j \in \mathcal{T}_s \quad (2.2.15)$$

$$z_i^m = z_j^m \quad \forall i, j \in \mathcal{T}, m \in \mathcal{M} \quad (2.2.16)$$

$$\sum_{m \in \mathcal{M}} z_i^m = 1 \quad \forall i \in \mathcal{T} \quad (2.2.17)$$

$$z_i^m + z_j^m \leq 1 \quad \forall (\{i, m\}, \{j, m\}) \in \mathcal{C}_{mm} \quad (2.2.18)$$

$$z_i^m = 0 \quad \forall (\{i, m\}) \in \mathcal{C}_{me} \quad (2.2.19)$$

Where z_i^m is the binary decision variable determining whether mooring design m from the set of available mooring designs \mathcal{M} is selected for turbine i , \mathcal{C}_{kk} is the set of IACs that cross each other, \mathcal{C}_{mm} is the set of mooring systems that have mooring lines that cross each other or anchors within 100 m of each other, and \mathcal{C}_{me} is the set of mooring systems that have an anchor outside of the domain or have an environmental obstacle between the anchor and the turbine. Constraints from Equation 2.2.3 to Equation 2.2.15 are taken directly from the WFCRP [16]. A constraint is added such that any two turbines must have the same mooring design in Equation 2.2.16. Furthermore, by Equation 2.2.17, every turbine must have exactly 1 mooring system in a single orientation. Equation 2.2.18 and establish that the mooring systems do not cross each other. Finally, Equation 2.2.19 establishes that mooring systems must have a feasible anchor location which is not outside the domain nor obscured by an obstacle.

The calculation of b_{ij} is unfortunately not trivial, as the shortest cable routing between a pair of turbines can be complicated, or even impossible. An algorithm has been proposed to solve this problem [48], which is in essence another optimisation problem nested within the FWFCRP. The requirements placed upon the IAC routing are twofold. First, they may not cross each other or mooring lines in the horizontal plane, as this would complicate installation and maintenance, greatly increasing costs. Second, there must be a separation of 100 m between anchors and an IAC, as well as a 10 m separation between two IACs or an IAC and a

mooring line or turbine, excluding when a connection is made [25]. This second requirement would usually be evaluated in 3-dimensional space, however, if two elements are only significantly separated vertically, any maintenance on the lower element will be challenging as this can not be done from right above it. Thus, this is also deemed undesirable and thus the evaluation purely in 2 dimensions is a reasonable assumption.

2.2. Mooring System Design Optimisation Problem

As discussed previously, the design of the mooring systems which will be used in the FWFCRP will be performed prior to the FWFCRP. The mooring system designs should comply with certain constraints to ensure that the turbine can function effectively throughout its entire lifetime and should result in the lowest costs for the overall farm. There are two elements to this cost minimisation. The first being the cost of the mooring system itself, and the second being the costs induced by the mooring systems on the IACs by requiring longer cable routes. While the costs induced by the mooring systems on the IACs are impossible to directly estimate without solving the FWFCRP, it is possible to use another metric to differentiate between mooring systems that is the main influence on these induced costs, being the anchor radius. The anchor radius, the horizontal distance between the anchor location and the equilibrium location of the centre of mass of the turbine-floater system with no external forces on the turbine-floater system and the mooring system, determines alongside the orientation of the mooring design the locations of the anchors and the paths taken by the mooring lines, and thus defines the obstacle that must be avoided in the cable routing, and an enlargement of this obstacle should generally increase the lengths of the IACs, increasing their costs. It can even be assumed that if the mooring radius is too large, it may not be possible to find a feasible cable routing at all. Thus, minimising the anchor radius is a key objective of the mooring design, alongside the minimising of the cost of the mooring system. Using a semi-taut mooring system design at a water depth of 56 m, it is found that the mooring system costs increased when the anchor radius was reduced below 300 m, and that a Pareto front is mapped when optimising in anchor radius-cost space [46]. Thus, as there is no known way to accurately weigh the anchor radius against the mooring system cost in terms of importance, a multi-objective optimisation must be used to find a range of Pareto-optimal mooring designs. While it is possible to use the vector length and angle in radius-cost space for optimisation [46], this was done to ensure a variety of solutions with a wide range of anchor radii were found. In a practical context, this is not necessarily desirable, as above a certain anchor radius, there are no longer significant savings in cost, and the costs may even increase due to the excessive length of the mooring lines. Thus, this choice will not be made in this thesis. Instead, the MSDOP will be formulated as follows:

$$\min C(\mathbf{x}) = (C_s x_2 x_4^2 + C_c (1 - x_2) x_5^2) \frac{\pi}{4} x_1 \sqrt{x_3^2 + h^2} + \frac{k_{a,1} f_{s,a} n_a}{k_{soil}} (\phi_1(\mathbf{x}))^{k_{a,2}} \quad (2.3.1)$$

$$\min x_3 \quad (2.3.2)$$

$$s.t. \quad x_1 - \frac{x_3 - R_f + h - h_f}{\sqrt{(x_3 - R_f)^2 + (h - h_f)^2}} \leq 0 \quad (2.3.3)$$

$$\phi_2(\mathbf{x}) \leq 0 \quad (2.3.4)$$

$$\sqrt{\phi_3^2(\mathbf{x}) + \phi_4^2(\mathbf{x})} - k_{s,max} h \leq 0 \quad (2.3.5)$$

$$\phi_5(\mathbf{x}) - \theta_{max} \leq 0 \quad (2.3.6)$$

$$h - 1 - \phi_6(\mathbf{x}) \leq 0 \quad (2.3.7)$$

$$\phi_9(\mathbf{x}) - \alpha_{max} \leq 0 \quad (2.3.8)$$

$$f_{s,T_m} \phi_{10}(\mathbf{x}) - 1 \leq 0 \quad (2.3.9)$$

$$\phi_7(\mathbf{x}) - k_{T,min} \phi_8(x_4) \leq 0 \quad (2.3.10)$$

$$-\phi_{11,\delta}(\mathbf{x}) \leq 0 \quad \forall \{\delta \in \mathbb{N}, \delta \leq 6\} \quad (2.3.11)$$

$$\phi_{11,1}(\mathbf{x}) - f_{1,max} \leq 0 \quad (2.3.12)$$

$$f_{1,min} - \phi_{11,1}(\mathbf{x}) \leq 0 \quad (2.3.13)$$

$$\phi_{12}(\mathbf{x}) - M_{TB,max} \leq 0 \quad (2.3.14)$$

Where \mathbf{x} is the vector of design variable, which are the mooring line length ratio, fraction of the mooring line length which is synthetic line (at unstretched conditions), anchor radius, diameter of the synthetic line,

Table 2.1: Outputs ϕ_i from RAFT simulations and analyses

Output number	Parameter
1	Maximum force at an anchor [N]
2	Binary variable denoting if the static RAFT analysis encounters an error [-]
3	Maximum FOWT surge displacement [m]
4	Maximum FOWT sway displacement [m]
5	Maximum FOWT pitch angle [°]
6	Maximum depth of the connection between synthetic line and chain [m]
7	Minimum static tension in a synthetic mooring line [N]
8	Minimum Breaking Load of a synthetic mooring line [N]
9	Maximum angle from the horizontal plane of force at an anchor [°]
10	Maximum ratio of tension to Minimum Breaking Load in a mooring line [-]
11	Eigenfrequencies of the system [Hz]
12	Maximum tower base moment [Nm]

and diameter of the chain, respectively. All the ϕ_i are outputs taken from either static or frequency-domain simulations of the model of the FOWT with a particular mooring design, and are listed in Table 2.1. It can be noted that the first of these is included in the objective function, being the maximum force applied to an anchor, used for the anchor sizing.

The approach taken here to use the design variable of having anchor radius be an optimisation objective is similar to the approach taken by West et al [46]. While on its own, Equation 2.3.2 is trivial, the minimisation of the radius leads to an increase in cost, and it is hypothesised that the usage of higher radius mooring systems will increase IAC costs. As the balance between these two contrasting objectives is unknown, the primary method to find the designs on this Pareto front will thus be a multi-objective optimisation with all mooring systems in the Pareto front used in the layout optimisation. However, a secondary methodology using a single objective optimisation will also be used to ascertain the performance of the multi-objective optimisation.

The cost function in Equation 2.3.1 is a direct function of all 5 design variables through the two terms that give the cost of the synthetic and chain sections of the mooring lines, as well as indirectly through the maximum anchor loading in the anchor cost term. The cost of connections between lines is not accounted for as these are the differences between designs in this aspect would be negligible, and they are usually not accounted for in other optimizations, such as by [46], [43], and [49]. The constants for the line costs are simply the cost per unit volume of the lines, while the anchor cost is computed using multiple factors, it is based on an empirical formula derived by [46] from data from Delmar Vryhof, with two constants that are anchor design dependent and one which is soil condition dependent. In addition, this is adjusted using the number of anchors and a safety factor from [50].

The constraints are all formatted as a condition being less than 0 for the purposes of the NSGA-II implementation. In Equation 2.3.3, the maximum length constraint can be seen. The line length ratio, which is defined as the ratio between the total length of the mooring line and the straight line distance between fairlead and anchor, should not be so large as to create a mooring line which can drop straight down to the seabed and then travel along the seabed to the anchor, as this will always provide insufficient stiffness. While this constraint is essentially redundant as any such mooring system will also violate other constraints, it does improve the performance of the algorithm by reducing the number of extremely unrealistic mooring designs for which more detailed simulations must be run.

In Equation 2.3.4, a binary variable for whether the RAFT static analysis encounters an error, such as a diagonal stiffness matrix of the system, which would indicate that the mooring system provides negligible stiffness and thus the equilibrium calculation becomes infeasible. This variable is 0 by default and 1 if the analysis encounters an error. This allows wider limits for the design variables to be set and thus not compromise the design space without mooring systems which are obviously unreasonable halting the optimisation or not being recognised as having constraint violations due to the inability to analyse them. Furthermore, in the static analyses already constraints Equation 2.3.5 through Equation 2.3.10 can be evaluated. These constraints limit the horizontal excursion, pitch angle, distance from the seabed of the synthetic lines, angle at which the force on the anchor is applied, maximum tension in all mooring lines, and minimum static tension in the synthetic lines respectively. Excluding the minimum static tension constraint, however, the driving factor for these

Table 2.2: Differences between frequency-domain FOWT models

Characteristic		RAFT	Wayman	Hall et al.	QuLAF
Hydrodynamics source		Integrated	WAMIT		
Aerodyn.	Contributions	A, B	B		
	Frequency dep.	Yes	No		Yes
	Source	Integrated	FAST		
	Control included	Yes	No		Yes
Mooring	Implementation	Quasi-static	Static	Quasi-static	Lin. of dynamic
	Source	Integrated		FAST	MoorDyn
Time-domain pre-processing		No			Yes

constraints is in dynamic simulations, so they will be discussed later. The minimum static tension constraint, Equation 2.3.10, is specific to only the synthetic sections of the mooring lines, and exists due to the detrimental effects of compression on synthetic lines, inducing much earlier failure. While this problem is less critical with the polyester lines commonly used in current mooring systems, it is nonetheless desirable to keep the mean tension above 2% of the minimum breaking load per [25].

Equation 2.3.11 through Equation 2.3.13 govern the eigenfrequencies of the system. Firstly, it is necessary that all eigenfrequencies are positive, as a negative eigenfrequency is again an indication of a very unrealistic mooring system in terms of its dynamic response, causing issues with RAFT's solvers. To ascertain whether the system has an acceptable range of stiffness, stricter requirements are set for the surge eigenfrequency [46], and thus limits are set that relative to the wave period are the same as in the study by West et al [46].

A number of the constraints limit the motions and loads on the system. This includes the aforementioned constraints in Equation 2.3.5 through Equation 2.3.9, as well as Equation 2.3.14. For the horizontal excursion, as this is a frequency domain analysis, it is not possible to find the combination of surge and sway that gives the largest excursion, so instead the maximum of each is combined for a conservative estimate. The limit for this constraint is set as a fraction of the water depth, as it is mainly determined by the inter-array power cable, specifically the amount of slack in it, which is usually accounted for as a percentage of the depth, per [23]. The maximum pitch angle is taken from [46], while the factor of safety on mooring tension is once again from [25]. Finally, the maximum tower-base moment is limited to be less than what was found in the load analysis of [11].

2.3. Mooring System Response Modelling

As shown in section 2.2, most constraint evaluations as well as the cost of the mooring systems requires inputs from simulations of mooring designs under particular loading conditions. These inputs will be taken from simulations using RAFT, developed by Hall et al. [41]. RAFT is a frequency-domain FOWT model which uses the quasi-static MoorPy model for mooring reactions. While frequency-domain tools are not as accurate as dynamic time-domain simulations, they provide the capability to analyse load cases much faster than time-domain solvers can, per [41], and thus are particularly suited to early phases of design and optimisation where multiple load cases must be analysed for hundreds of different designs to be able to judge their performance. RAFT, however, is not the only such model, with others including the model proposed by Wayman [51], an earlier model by Hall et al. [52], and QuLAF [35].

While all 6 models assume linearity and make use of the same generic equation of motion in the frequency domain, shown in Equation 2.4, the differences mainly lie in how the coefficient matrices that determine the system characteristics are calculated. As shown in Table 2.2, RAFT is unique in including the aerodynamic component of added mass, as well as allowing control and frequency dependent aerodynamics without requiring pre-processing in time-domain. Furthermore, RAFT does not require pre-processing with other software such as FAST or WAMIT, as the aerodynamic, hydrodynamic, and mooring calculations are done by the integrated packages CCBlade, HAMS, and MoorPy [42].

$$(\omega^2 (\mathbf{M} + \mathbf{A}(\omega)) + i\omega\mathbf{B}(\omega) + \mathbf{C}) \hat{\xi}(\omega) = \hat{f}(\omega) \quad (2.4)$$

In terms of validation, while Wayman and Hall et al do not mention how their models perform when compared against a time-domain model such as FAST, RAFT and QuLAF are both verified with FAST. In terms of

natural periods, QuLAF has an error of 0.0% relative to FAST in surge, 0.4% in heave, and 1.3% in pitch, on the FOWT tested. Meanwhile, RAFT has a maximum errors of 15.2%, 3.4%, and 5.8% respectively over 3 tested FOWTS. Similarly, QuLAF qualitatively shows a better agreement with FAST in the power spectral densities of the responses to irregular waves. Thus, clearly, QuLAF has a stronger agreement with FAST than RAFT. However, it was not chosen for this research because of the time-domain pre-processing needed not just for the aerodynamics of the turbine, which in a mooring optimisation context would only have to be performed once, but more so for the pre-processing needed to run the 7 MoorDyn simulations for each mooring design necessary to linearise the mooring system at the extreme wind speed. This would be prohibitively expensive for computation, and thus it was chosen to move forwards with RAFT.

RAFT uses a slightly expanded form of the generic equations of motion for the dynamic response, which is shown in Equation 2.5 in addition to the static equilibrium equation shown in Equation 2.6, as per [41]. While these equations are linear, some of the dependencies on frequency are not, which is accounted for in an iterative solution of the response amplitudes. RAFT assumes rigid body dynamics, computed in 6 degrees of freedom. The mooring system data is passed through the quasi-static solver MoorPy, along with the hydrostatic stiffness of the FOWT and the applied loading conditions. MoorPy can then solve for the equilibrium position and forces in each line as well as the stiffness of the mooring system about this point. Furthermore, MoorPy also solves for a Jacobian of the mooring line tensions to allow for estimation of mooring dynamics. Finally, RAFT uses a strip-theory approach to solve the hydrodynamics, as well as a steady-state blade element momentum solver to compute the steady-state aerodynamic forces and moments, as well as their derivatives. In this thesis, the option to enable control is also included where relevant, and thus RAFT will also calculate fluctuations in the rotor speed and blade pitch and their contributions to the system dynamics.

$$(\omega^2 [\mathbf{M}_{struc} + \mathbf{A}_{sub}(\omega) + \mathbf{A}_{aero}(\omega)] + i\omega [\mathbf{B}_{sub}(\omega) + \mathbf{B}_{aero}(\omega)] + \mathbf{C}_{struc} + \mathbf{C}_{moor}) \hat{\xi}(\omega) = \hat{f}(\omega) \quad (2.5)$$

$$\mathbf{C}_{struc} \bar{\xi} = \bar{f}_{aero} + \bar{f}_{hydro} + \bar{f}_{moor}(\bar{\xi}) \quad (2.6)$$

2.4. Multi-Objective Mooring System Optimisation Methods

The nondominated sorting genetic algorithm II (NSGA-II) is an algorithm which allows for multiobjective optimisation in a manner that is fast, allows to keep the best performing individuals in the tested population without mutation, and does not require any parameters to be specified to guide the maintaining of diversity in solutions [53]. This algorithm focuses on the concept of domination, where one solution is dominated by another if the latter improves on the former in both objective functions. This creates fronts, or sets of solutions, which have common domination characteristics. The front which is entirely nondominated, is known as the Pareto front, with any individual included being considered Pareto-optimal. A Pareto-optimal solution is one which is not dominated by any other, and thus no solutions exist which outperform it in both objective functions. Further fronts are formed by solutions which are dominated solely by individuals in prior fronts. Thus, for example, the second front contains solutions which are dominated by some others, but only those which are within the first front. In NSGA-II, this is done by comparing each solution to every other and saving two pieces of information. The first is the number of solutions the one of interest, the domination count, and the second is the list of solutions that the one of interest dominates, the domination set. This allows for the formation of fronts beyond the first without having to compare the solutions again, by subtracting from the domination count for any individual which is included in the domination set of a individual from the previous front. As the domination sorting is the most complex part of the algorithm, this reduces the complexity of NSGA-II compared to earlier attempts from $O(MN^3)$ to $O(MN^2)$.

Rather than using a sharing function with a user-defined parameter, NSGA-II uses a crowding distance metric to maintain diversity in the solution population. The crowding distance is estimated as the absolute difference in objective function values between the two adjacent solutions on the same front, with those on the ends having an infinite distance. The solutions are then ordered first by lowest nondomination rank, and then by highest crowding distance. In each generation, the old and new population are combined and ranked and only the highest ranked half is then used to create a new population as in any genetic algorithm using tournament selection, recombination, and mutation, with the compound domination and crowding rank being used for the tournament selection. Over a variety of test problems, this algorithm showed marked improvements in convergence after a set number of generations, indicating its speed and accuracy at finding optimal solutions, as well as in the diversity of the solutions found.

Table 2.3: Overview of constraints by tiers

Step of Evaluation	Constraints Evaluated
Geometric	2.3.3
Static	2.3.4, 2.3.5, 2.3.6, 2.3.7, 2.3.10, 2.3.8, 2.3.9
Eigenvalue	2.3.11, 2.3.12, 2.3.13
Load case	2.3.5, 2.3.6, 2.3.7, 2.3.8, 2.3.9, 2.3.14

Despite the NSGA-II algorithm converging quickly to the set of Pareto-optimal solutions, the nature of the MSDOP means that many designs must be tested, and many will not pass the constraints. Each analysis of a design requires multiple RAFT simulations to establish constraint compliance, and this can take significant computational time. Thus, similar to [46], a tiered constraint system was used, in order to not evaluate computationally expensive constraints if earlier constraints have already been violated. Constraints are evaluated in a number of steps, being split into geometric, static, eigenvalue, and extreme load case constraints, as illustrated by Figure 2.1. The anchor cost can only be computed using data from the extreme load cases, thus the system cost is set to 0 if the design is infeasible to prevent an incomplete comparison occurring if infeasible results must be sorted. An overview of which constraints are evaluated at which step can be found in Table 2.3.

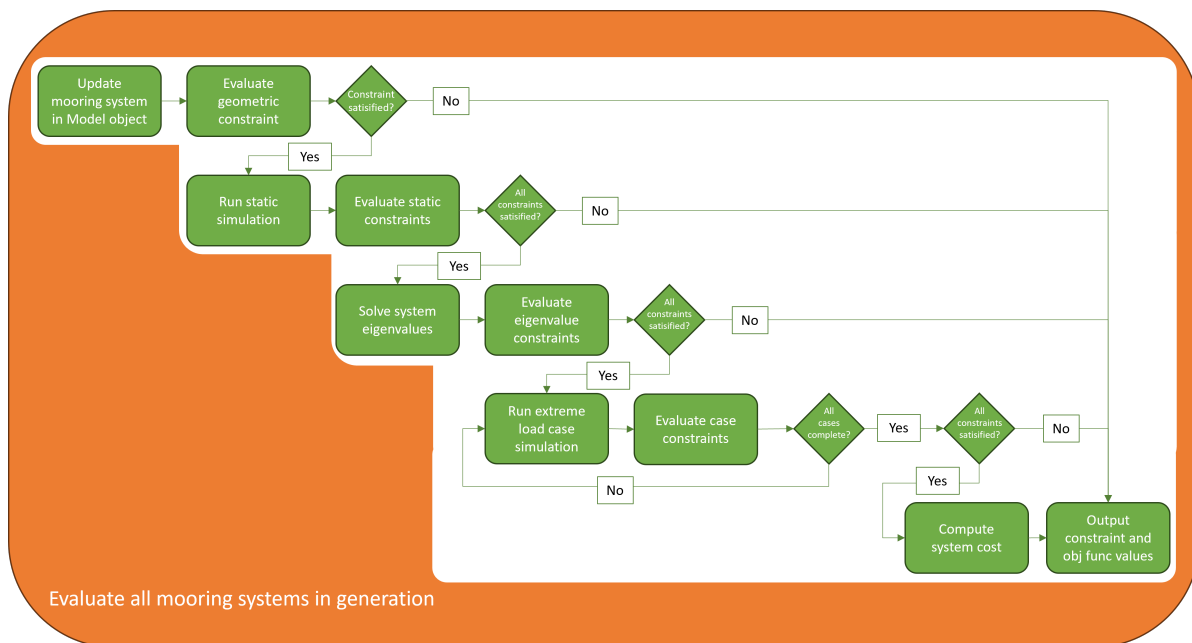


Figure 2.1: Flowchart of the tiered constraints system

2.5. Single-Objective Mooring System Optimisation Method

For the single-objective optimisation, the aim was to have the least possible differences to the multi-objective method. Thus, a genetic algorithm was also chosen, and the same methods of crossover and selection were used as in the NSGA-II algorithm. Furthermore, the optimisation problem was also largely kept the same, with the same design variables, cost function, and constraints. The only difference is that the radius was now used exclusively as a design variable, rather than as both a design variable and an objective function. A series of single-objective optimisations was performed, with the anchor radius domain split into slices of 25 m. Within each slice, an optimisation was performed, thus there was still variation possible in the anchor radius within each optimisation. In order to increase the performance of the algorithm, the final generation of each optimisation problem was used to form the zero-th generation of the next optimisation problem. The first optimisation was chosen to be the geometric average of the two anchor radius limits, as feasible solutions were obtained more swiftly in this range rather than towards the extremes of the design space, thus

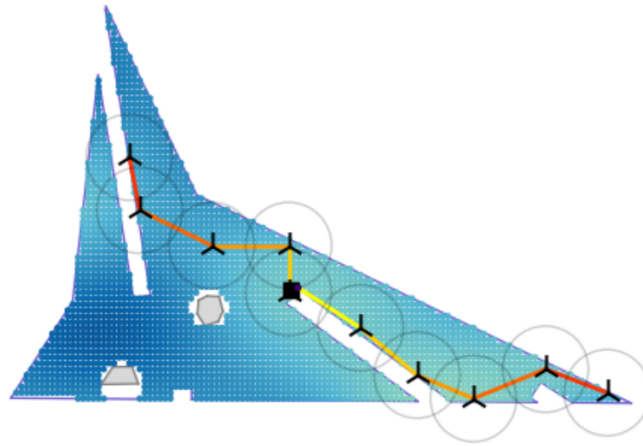


Figure 2.2: A proposed layout from the research of Cazzaro [16] for one area of instance C

it would still obtain good results quickly without the use of a biased initiation. From there, two sequences of optimisations were performed, one increasing the anchor radius up to its maximum, and one decreasing the anchor radius to its minimum. To create the biased initiations for the subsequent optimisations, the anchor radius of the last generation of the previous optimisation was adjusted to fit within the new bounds, and then the designs were re-evaluated with the new anchor radii. While these designs generally did not perform as well as the designs from which they were taken, it is nonetheless an improvement over random initiation.

2.6. Layout Optimisation Methods

As previously mentioned, the layout optimisation is performed in two stages, and thus this method can be split into two distinct phases. First, the CWFOP is solved to find the optimal turbine locations. Second, the FWFCRP is solved to find the optimal mooring designs and cable routing.

First, the CWFOP is solved as it is by Cazzaro [16], which contains a number of steps. First, turbines are placed at all possible locations defined in the grid. The influence of any turbine on any other turbine in terms of wake losses is pre-computed using a custom wake model property of Vattenfall AB, and iteratively the turbine that has the worst combination of losses experienced and losses caused for other turbines is removed. A penalty is added for turbines which violate the minimum distance constraint to another turbine. Once the desired number of turbines is obtained, it is checked whether the initial solution violates the minimum distance constraint. If it does not, the solution is repaired using a greedy constructive heuristic. To then obtain the initial solution for the cable routing, the turbines are separated a number of groups by the angle of the vector from the substation to the turbine. The number of groups is defined by the number of cables that can be connected to the substation. This method allows a minimal likelihood of crossing cables. Within each group, due to the low number of turbines (usually 7 or less), every possible order of turbines to connect can be evaluated. This then gives an initial solution for the turbine layout and the cable routing.

An important difference between the CWFOP as presented in earlier research and how the problem is solved for this thesis, is how the domain for turbine placement is determined. In the algorithm as proposed by Cazzaro, turbines can be placed anywhere within the farm boundary area, excluding where obstacles are placed. However, as seen in Figure 2.2, this can lead to turbines being placed very close to the substation, which due to the lack of power losses caused by the substation and the obviously low cable length associated with this placement is often quite advantageous. This is unrealistic even for bottom-fixed farms, as the proximity of the blades and the substation could cause damages through a strike. However, for floating wind farms, the proximity of the turbines to the substation leads to a lack of a feasible solution to the cable routing problem in many cases. This is due to the proximity of mooring lines and anchors to the substation, which cannot be crossed or approached respectively by IACs. To resolve this issue, a safety zone surrounding the substations is considered, meaning no turbines can be placed within 500 m plus the anchor radius of the mooring system, leaving enough space for multiple IACs to connect to the substation.

Once this initial solution has been computed, the algorithm proceeds as in the work by Cazzaro [16], with a

VNS method. In the VNS, two stages are alternated. The first is a combined local search, where the layout of the wind farm is changed in a minor way, and the change in NPV between the different options is computed. The NPV is computed as shown in Equation 2.1.2. If a change improves the NPV and does not violate one of the constraints, it is kept. Two types of changes are possible. The first consists of moving one turbine a small distance and computing the changes in cable lengths and wake losses from this turbine. The second consists of moving two nearby turbines simultaneously and then doing the same computations. The second stage consists of moving a larger subset of turbines randomly to nearby locations, while still maintaining feasibility. This is to enable the optimisation to escape local optima. After each phase, the cable routing is recomputed using the same method as for the initial solution, in order to ensure that the cable routing is always optimal for the current solution, and that the layout is not restricted by the initial cable routing solution. Once both the 1 and 2 turbine moves fail to return improvements for all turbines, the optimisation terminates.

2.7. Case Study

In order to investigate the effect of integrating mooring design with the wind farm design optimisation, the algorithms devised will be tested on a synthetic wind farm instance based off of [54]. Specifically, instance B will be used, as it is the smallest site which is not split into two domains. As this site is rather small, it should reduce the computational time of the optimisation due to a smaller number of possible turbine positions. One adjustment will be made from this synthetic instance, which is the water depth, as the instance specifies water depths varying between about 10 and 40 m, which is not a realistic depth for industrial-scale floating wind farms, and thus may cause issues with finding suitable mooring systems. Instead, it was assumed that the water depth was constant at 105 m throughout the site. This depth was chosen as it is approximately the average water depth of demonstrator project presented by [26]. The choice to assume a constant water depth was made to reduce the computational time and complexity of the mooring design optimisation problem. A range of water depths would require double the number of simulations run, as each constraint must be evaluated on both the minimum and maximum water depth.

Other features of the case study are chosen to facilitate comparison to [16]. Thus, the turbine used will be the IEA 15 MW turbine [11], as this turbine also has an associated established semi-submersible floater designed for it, the VoltturnUS-S [12], as used in [46]. Similarly, the metocean data parameters will be taken from public measurements at the Ten Noorden van de Waddeneilanden wind farm site in the Netherlands [55]. A variety of power densities will be used, to analyse the effects of different turbine densities on which mooring systems are preferred in the optimisation. Soil conditions will initially not be included in the case study, as their application relates only to a more accurate cost estimation for the anchors. Furthermore, the mooring systems investigated in the case study will initially be limited to catenary mooring systems. For catenary mooring, a combination steel chain and polyester line is generally preferred, however, there are multiple different grades of chain. The preferred grade in industry is generally R3 Studless chain, due to the low cost. The key parameters relating to this type of chain and polyester lines are presented in Table 2.4 [31]. Furthermore, the anchor used to estimate costs will be the Vryhof Stevmantis Mk 5 [46], a drag embedment anchor, and the soil constant used in [46] will be taken to be 50, similar to in that paper. The mooring designs investigated will also have rotational symmetry and have 6 mooring lines grouped into 3 legs, meaning that each line will have the same length and anchor radius, and that the lines will have a 115° offset from the adjacent line in another leg and a 5° offset from the adjacent line in the same leg. This is illustrated in Figure 2.3.

Table 2.4: Key parameters of the different line types relative to the nominal diameter d_c [mm] [31]

Parameter	R3 Studless Chain	Polyester
Minimum breaking strength [kN]	$22.3d_c^2(44 - 0.08d_c)$	$250d_c^2$
Submerged weight per unit length [N/m]	$0.171d_c^2$	$0.0017d_c^2$
Axial stiffness [GPa·m ²]	$85.4d_c^2$	$1.1d_c^2$
Transverse added mass [-]	2.0	1.0
Tangential added mass [-]	1.0	0.1
Transverse drag [-]	2.4	1.6
Tangential drag [-]	1.15	0.1
Cost [\$/kg]	1.5	17

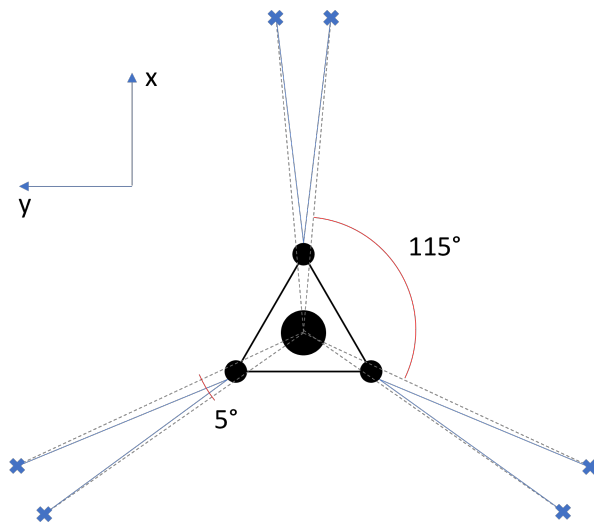


Figure 2.3: Illustration of the mooring system configuration

3

Results and Discussion

3.1. Mooring System Optimisation

3.1.1. Extreme Load Case Analysis

In order to ensure the optimisation process is efficient while still being conservative, a preliminary analysis was carried out to ascertain which extreme load cases were necessary to evaluate. The evaluation of extreme load cases is by the most computationally intensive process in the optimisation, thus cutting down the number of evaluations is critical to improve the performance and feasibility of using the optimisation. The extreme load cases are defined by 12 parameters, of which 5 are varied across different load cases. An overview of the 7 parameters which are not changed is given in Table 3.1. As mentioned previously, all metocean data used here is from the Ten Noorden van de Waddeneilanden wind farm zone [55]. The wind speed and current correspond to the 50-year omnidirectional maximum that can be expected at the site. As the wind speed used is above the cut-out wind speed of the turbine, it is simulated in a parked state. For simplicity, it was assumed that the rotor plane was always perpendicular to the wind direction and that there was no turbulence in both wind and current.

Table 3.1: An overview of the load case parameters used for all possible load cases

Parameter	Value
Wind Speed	41.5 m/s
Wind Turbulence Intensity	0
Turbine status	Parked
Yaw Misalign	0
Wave Spectrum	JONSWAP
Current Speed	1.1 m/s
Current Turbulence Intensity	0

The 5 load case parameters which are varied were the heading of the wind, wave, and current relative to the mooring design (simply referred to as the heading for the rest of this thesis), as well as the wave conditions in height and period. The combinations of wave period and height used correspond to the 50 year extreme wave height and the wave period associated with it, however 5 directional extremes were used rather than the omnidirectional maximum. The reason for this is that the periodic nature of the wave loading may cause a resonant response, and thus it is desirable to investigate extreme wave heights with a slight range of associated periods. The list of directional extreme wave conditions used is shown in Table 3.2. The headings used also were considered as the two extreme cases, being a heading of 0° or a heading of 60° . The headings are defined as the direction from which the metocean phenomenon originates, such that a wind heading of 0° would constitute wind coming from the positive x direction. As shown in Figure 2.3, a heading of 0° would introduce a load which is aligned with the midline of one of the legs, while a heading of 60° would introduce a load that is right between two legs, thus constituting the two most extreme alignments. In order for the mooring systems to be able to be deployed in any orientation, all combinations of wind, wave, and current heading

are used at this stage. This is a conservative approach, as the extreme wind, wave, and current headings are not independent of each other, and thus are likely to be more aligned than is assumed here. Thus, with 5 sets of wave conditions and 3 phenomena with 2 possible headings each, 40 different cases are considered.

Table 3.2: Directional extreme wave conditions used for load cases

Cardinal Direction [°]	Wave Height [m]	Associated Wave Period [s]
360	7.2	12.8
330	9.2	14.1
300	8.8	12.8
270	7.9	11.7
240	7.1	10.9

To analyse which of these load cases are relevant, the optimisation was performed with all 40 cases simultaneously active, and constraint violations for each load case were tracked. Importantly, the tiered constraint system was altered for this simulation such that the evaluation of load cases would not be stopped if one load case evaluation produced constraint violations, but rather all extreme load cases would always be evaluated if the previous stages produced no constraint violations. The initial random population was set to 100 rather than 1000 for this simulation, and only 1000 designs were evaluated in total, due to the significant computational time associated with evaluating designs over 40 different load cases. Proceeding through 10 generations of optimisation makes for a more efficient process, as a higher proportion of designs tested will be realistic and pass through the earlier tiers of constraints, however this does mean that the designs are not all independent of each other and may thus exhibit some common characteristics which could cause similar constraint violations. If more time were available, it would be preferable to use a larger population of only randomly generated designs for this analysis. Nevertheless, the analysis is valuable to give an indication of which load cases are critical and thus what to prioritise in larger simulations. For the load case analysis, in order to distinguish which load cases are critical, the designs which produce constraint violations for some but not all cases are key. Designs which violate the geometric, static, or eigenvalue constraints are not worth evaluating, as they will be filtered out in a full optimisation as well and they are expected to violate constraints in most if not all extreme load cases. Obviously, if there are no constraint violations in the extreme load cases or if there are violations in every load case, then these designs do not provide any differentiation. The breakdown of how many designs are thus useful for the analysis and for what reasons the others are discarded is illustrated in Figure 3.1. As shown, out of the 1000 designs that are evaluated, only 70 are relevant in this case.

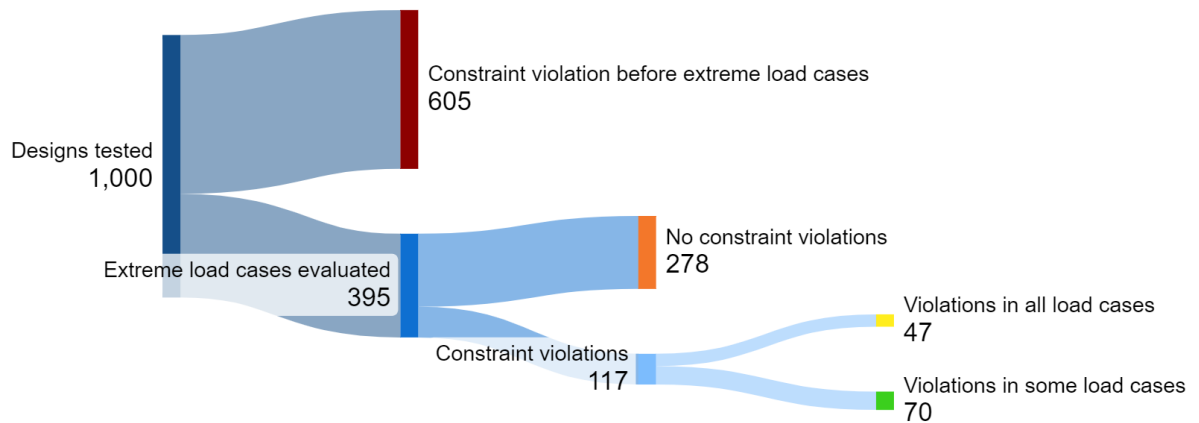
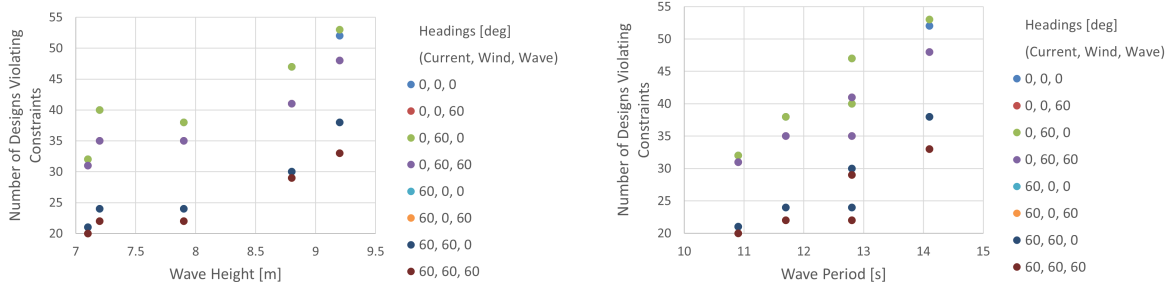


Figure 3.1: Sankey Diagram of outcomes of designs for the load case analysis

When examining the results from these 70 designs, a key metric to determine which extreme load cases are critical is the number of designs for which constraint violations occur for a particular load case. In Figure 3.2, it can be seen that each load case produces constraint violations for between 20 and 53 designs, or between

28 and 76% of the relevant designs. Clearly then, more than one extreme load case will be necessary to sufficiently constrain the design space. It can also be seen that both wave height and wave period have a positive correlation with constraint violations. This suggests that resonance issues are not common enough to be a major concern, meaning it is not necessary to further constrain the natural frequencies of the system as is done in another study [46].

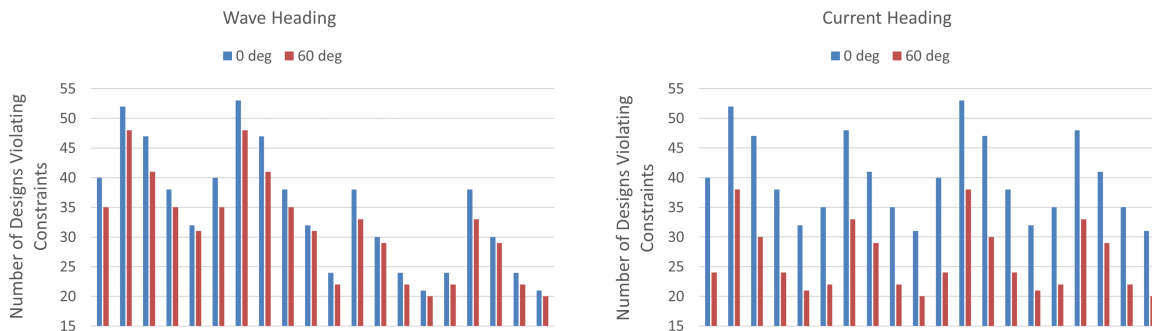
Beyond this, one would expect the higher wave amplitudes and periods to indeed lead to more constraint violations, as the forces imparted on the system are both larger and are applied in the same direction for a longer time. Out of the 6 constraints evaluated for extreme load cases, being the horizontal excursion, pitch angle, depth of the chain-synthetic line connection, angle of force at anchors, mooring line tension, and tower-base moment, that particularly the line tension and horizontal excursion should strongly correlate to increased wave height and period, as these are most directly linked to the loading imposed on the system.



(a) Plotted by wave height

(b) Plotted by wave period

Figure 3.2: Frequency of constraint violations for each load case



(a) For difference in wave heading

(b) For difference in current heading

Figure 3.3: Side by side comparison of constraint violations for load cases with only a heading difference in sea conditions

Furthermore, constraint violations are most common across all wave heights and periods for load cases with current and wave headings of 0°. This is more clearly shown in Figure 3.3. For every load case with a 0° current or wave heading, if only this heading is changed, the number of constraint violations decreases. It is clear that the current heading is more impactful than the wave heading, causing much larger decreases of 34.2% on average in comparison to only an 8.7% decrease when the wave heading is changed to 60°. This is to be expected, as waves are a sinusoidal phenomenon and thus a significant amount of the loading imparted on the structure is in the negative direction. Due to rotational symmetry, loading in the negative direction for waves from a 0° heading is equivalent to loading in the positive direction for waves from a 60° heading, and vice versa.

Interestingly, as shown in Figure 3.4, this relationship of more stress on the system with a 0° heading does not extend to the wind heading. Here, it can be seen, that for all but one of the 0° cases, changing the wind head to 60 does not change the number of designs which violate constraints. The only exception is for the two cases with the extreme wave conditions corresponding to a cardinal direction of 330°, and a heading of 0° for the waves and current. Here, there is a single constraint violation which differs, which is that the

mooring line tension constraint is violated for one design when there is a 60° wind heading but not for 0°. The mooring line tensions are 140% and 93% of a mooring line’s minimum breaking load accounting for safety factors. On average over all designs for which the extreme load cases are evaluated, the absolute value of the difference between the two load cases is about 0.27% of the minimum breaking load, with 16 out of the 395 designs showing a difference of more than 0.1%, split evenly between situations where the 0 and 60° load cases have larger mooring line tensions. The difference seen for the design in question is one of the largest of any design, and given this and the generally small difference between the two results, which is also not biased significantly towards either load case, this can be considered an outlier.

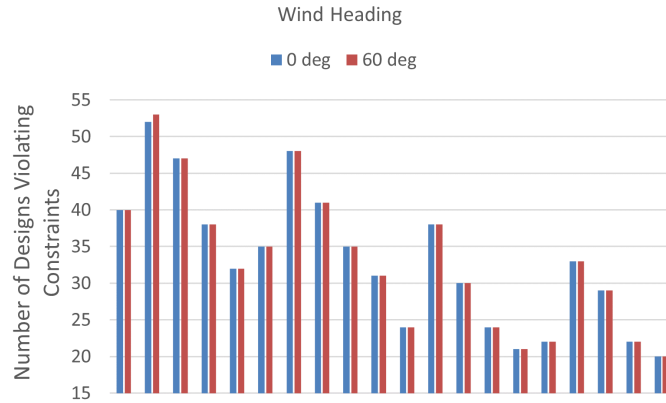


Figure 3.4: Side by side comparison of constraint violations for load cases with only a wind heading difference

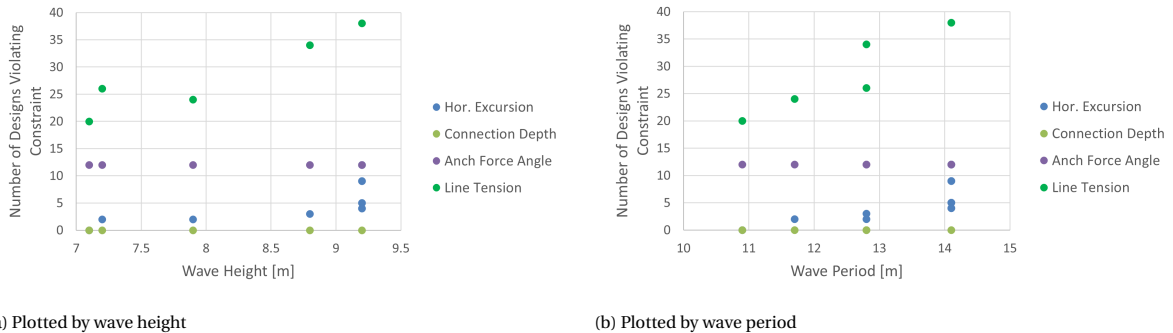


Figure 3.5: Frequency of violations of the constraints on horizontal excursion, force angle at anchor, and mooring line tension for load cases with 0° current and wave headings and a 60° wind heading

An analysis into which constraints are violated shows that the constraints on pitch angle and tower base moment are not violated for any design-load case combinations. For the load cases with 0° current and wave headings, which as mentioned earlier produce higher numbers of constraint violations, as well as arbitrarily choosing a 60° wind heading, the 4 constraints which do produce violations are presented against the wave height and period in Figure 3.5. As previously hypothesised, it can be seen that the violation of the horizontal excursion and mooring line tension constraints is heavily dependent on the wave height and period. The angle of force at the anchor and depth of the synthetic-chain line connection, on the other hand, is not affected by the wave height or period. In fact, the connection depth constraint is not violated for any of these load cases.

As shown in previous data, no load case produces violations in more than 53 of the 70 designs that produce violations on some but not all extreme load cases. This means that at least 2 load cases will be necessary to cover all constraint violations. As the load cases with the maximum wave height and period and 0° wave and current headings produce constraint violations for the most designs, one of the load cases with this combination of parameters will be chosen first. While previous analysis has suggested that the one constraint violation for the load case with these parameters and a 60° wind heading that is not present with the 0° wind heading is

an outlier, there is no other reason that would sway the choice between these two load cases. Thus, the load case with a 60° wind heading is chosen.

There are 17 designs which do not produce a constraint violation for this load case, but do for other load cases. All 17 of these designs produce constraint violations for at least the following two load cases. These load cases also have the maximum wave period and height, but have wave and current heading of 60°. The only difference is the wind heading, which as established previously does not make a difference in the number of designs with constraint violations. The main difference between the constraint violations for these designs and the constraint violations for the other 53 which have been covered by another load case, is that these designs all violate one of two constraints, the depth of the synthetic-chain line connection and the horizontal excursion, with 11 and 6 respectively. For the sake of completeness and redundancy, the one design which produces different results depending on the wind heading was also checked against both these load cases, for which it also produces constraint violations, though for the mooring line tension constraint, unlike the rest. As both load cases have the exact same constraint violations for every design, the choice between them is arbitrary, and a wind heading of 0° is chosen to be used in the rest of the simulations. The parameters of the two load cases used further are shown in Table 3.3.

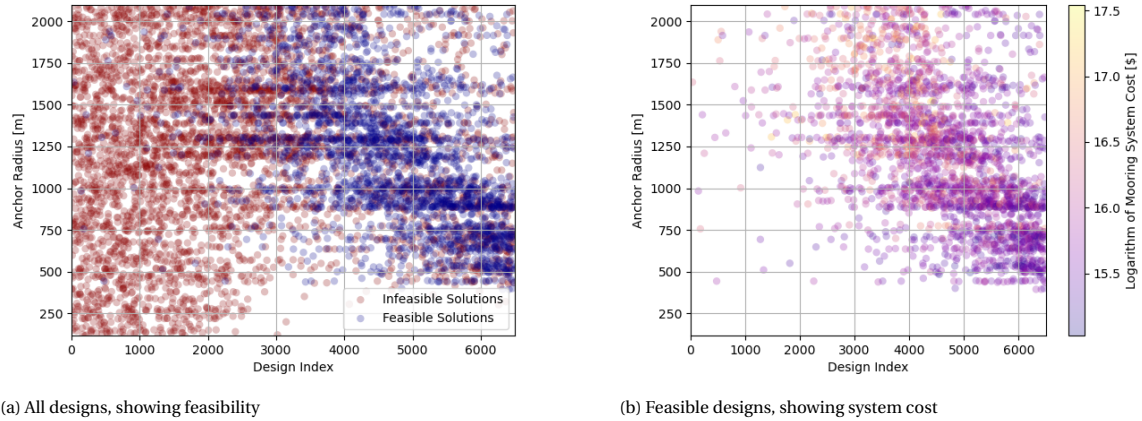
Table 3.3: Parameters of the Critical Load Cases used in further simulations

Parameter	Load Case 1	Load Case 2
Wave Height [m]	9.2	
Wave Period [s]	14.1	
Wind Heading [°]	60	0
Wave Heading [°]	0	60
Current Heading [°]	0	60

3.1.2. Multiple Objective Optimisation Progression

In the multiple objective optimisation, the progression of designs and the optimisation can be tracked using the index of each design. The index simply tracks the order in which designs are evaluated. As the initial randomly selected population consists of 1000 designs, and each subsequent generation of designs consists of 100 individuals, the generation to which each design belongs can be inferred from the index, with an index of less than 1000 meaning the design belongs to the initial population, and each subsequent increase of 100 in the index signifying the next generation. Knowing this, the progression of the distribution of each design variable can be tracked, and the feasibility and cost of designs along with them.

The first design variable that will be investigated is the anchor radius, given its dual function as a design variable and an optimisation objective. All else being equal, given that the line length is defined relative to the anchor radius, a higher anchor radius should result in an increased cost. However, it should also allow for a wider range of designs to be feasible, which could lead to lower costs options being available. The relevant constraints in particular, are those of The feasibility of designs is shown in Figure 3.6a. Immediately, it is clear that the majority of the design space is infeasible, as there are very few feasible solutions with a design index below 1000, where the designs are chosen at random. However, after this the rate at which feasible results are discovered rapidly increases, until after about design index 3000, representing generation 20, where a significant proportion of designs is found to be feasible. This is further shown in Figure 3.7. As shown, initially less than 5% of designs is found to be feasible, and this initially increases quite slowly. This can be attributed to the optimisation algorithm using the top 100 best designs so far, according to the criteria explained in section 2.4, to create the new population, which will initially include many infeasible designs, thus leading to a high probability of further infeasible designs. Once 100 feasible designs have been found after generation 14, the feasibility rate quickly grows. However, it is notable that once the feasibility rate reaches around 0.7, it stagnates, and even slightly decreases on average in subsequent generations. While at this point the population of parent solutions used consists of feasible solutions that give a high probability of providing new feasible solutions, there is still a sizeable fraction of infeasible designs created. This suggests that either there is significant diversity in the parent population, or that the parent population largely consists of individuals that are close to the limit of feasibility. Both of these options are desirable effects for the optimisation to exhibit, but it can based on this data not be ascertained which effects are present or dominant.



(a) All designs, showing feasibility

(b) Feasible designs, showing system cost

Figure 3.6: Progression of Anchor Radius

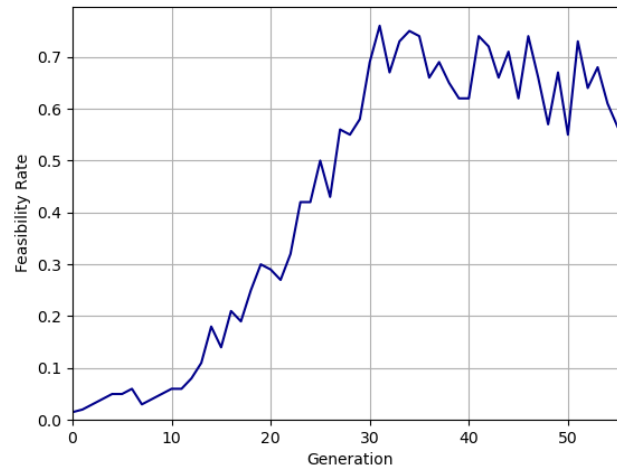


Figure 3.7: Proportion of solutions found that are feasible per generation

What can further be noticed from Figure 3.6, is that no feasible designs are ever found with an anchor radius below around 400 m. This leads to the design space that is explored being restricted after about 2500 designs. In similar studies [45], [46], the lowest radius options are at 235 m and 278 m, with water depths of 55 m and 56 m respectively. Thus, given that the water depth in this study is about 90% higher, it seems reasonable that the lowest radius options are between 40 and 70% higher. This means that the smallest radius designs in this study actually have a steeper average gradient than in previous studies, which suggests that the optimisation procedure is indeed finding results that are on the bounds of the feasible region of the design space. Furthermore, as the feasibility rate crosses 50% around generation 25 or design index 3500, it can be seen that the anchor radii in the population start to decrease towards the minimum value mentioned above. This can be seen in more detail in Figure 3.8. Clearly, the anchor radii initially spans the entire domain of the design variable, with a uniform distribution as one would expect from random initiation. However, from this initial value, as the feasibility rate starts to rise so too does the median and first quartile of the anchor radius. It can be seen in Figure 3.6 that there are more feasible designs found towards the high end of the anchor radius domain, as expected, which leads to more high radius designs in the parent population in the initial phases, driving up the median radius. However, the stabilisation of the feasibility rate at around 0.7 coincides almost exactly with a reversal in the changes to the median anchor radius. While the maximum radius stays largely unchanged, and the minimum increases to around 350 as mentioned previously, the first and third quartile and the mean radii decrease significantly beyond generation 30. From Figure 3.6b, it can be seen that as the algorithm progresses, costs savings are found both with increasing generations at a similar radius as well as

with decreasing radius at a similar design index. Thus, the low cost-low radius designs tend to dominate the low cost-high radius designs in the optimisation, leading to a reduction of high radius designs and an increase of low radius designs in the parent population. The reduction in mean radius once a significantly high portion of new designs are feasible thus follows the expectations, that high radius designs are more likely to be feasible but if a similar design with lower radius is feasible it will be cheaper. This has the result of dividing the optimisation into two clear phases, the first being to find the region of feasibility in the design space, and then the second to test the borders of the feasible region with cheaper and lower radius designs.

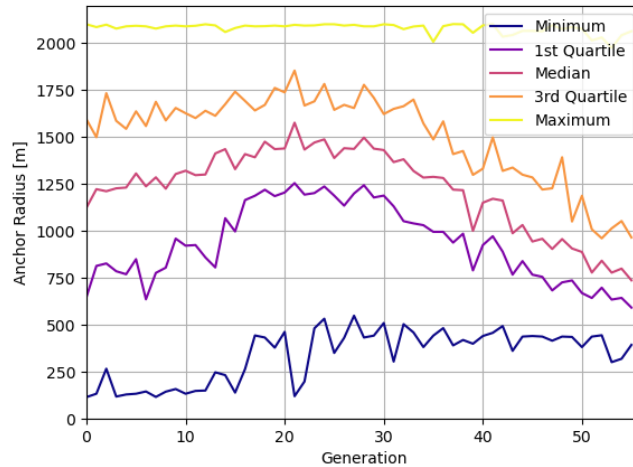
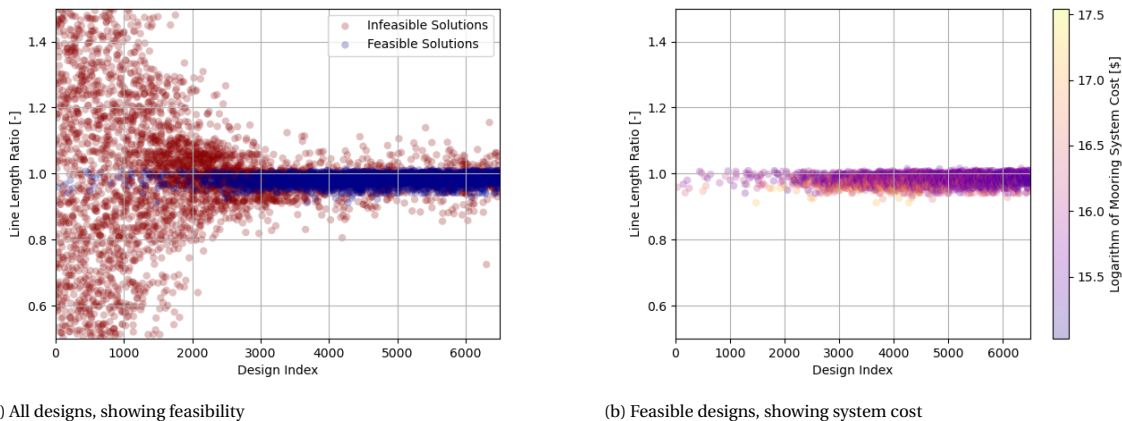


Figure 3.8: Quartiles of anchor radius per generation



(a) All designs, showing feasibility

(b) Feasible designs, showing system cost

Figure 3.9: Progression of Line Length Ratio

The next design variable to examine is the line length ratio, shown in Figure 3.9. The initial domain given is quite wide, and it is quickly clear that outside a narrow range, no feasible solutions are possible. This results in a significant reduction of the design space that is used, which is complete after about 10 generations. This is another significant factor in the increase of the feasibility rate from this point onwards. When investigating only the range in which feasible results are found between 0.91 and 1.02, as shown in Figure 3.10, it can be seen that designs closest to 1 have the highest rate of feasibility. This is not unexpected, as these designs have to no slack in the line when not forced, but also do not have any extra pre-tensioning outside the effects of gravity which pull the line into a catenary shape. Thus, it strikes a balance between minimising the tension in the mooring lines while not allowing excessive excursions or violating the constraint on the minimum pre-tension in the synthetic lines. As the differences in absolute line length resulting from the changes in line

length ratio seen are rather small, only about 45 m for the median design in terms of anchor radius in the final generations using the main range of feasible results from 0.95 to 1.01, this does not have a large effect on the mooring system cost for designs of a similar generation, as shown in Figure 3.10b.

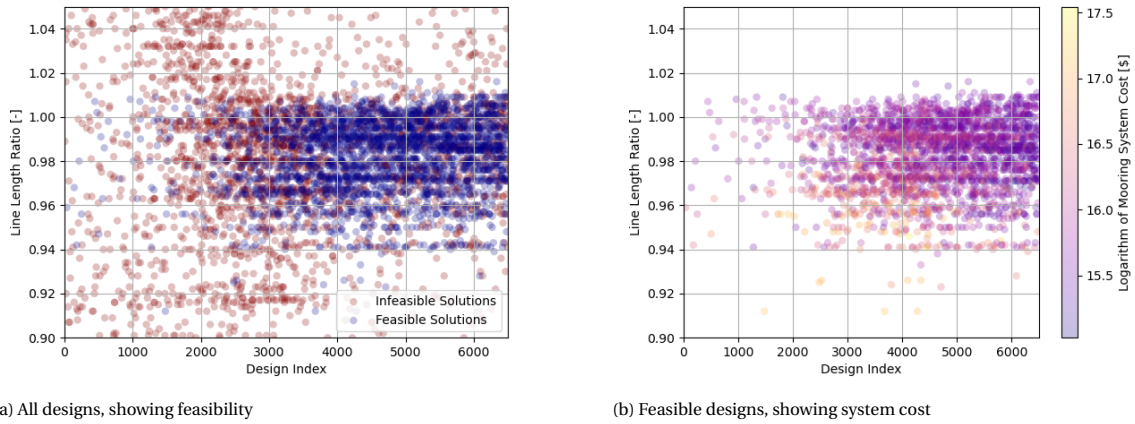


Figure 3.10: Progression of Line Length Ratio shown on reduced domain

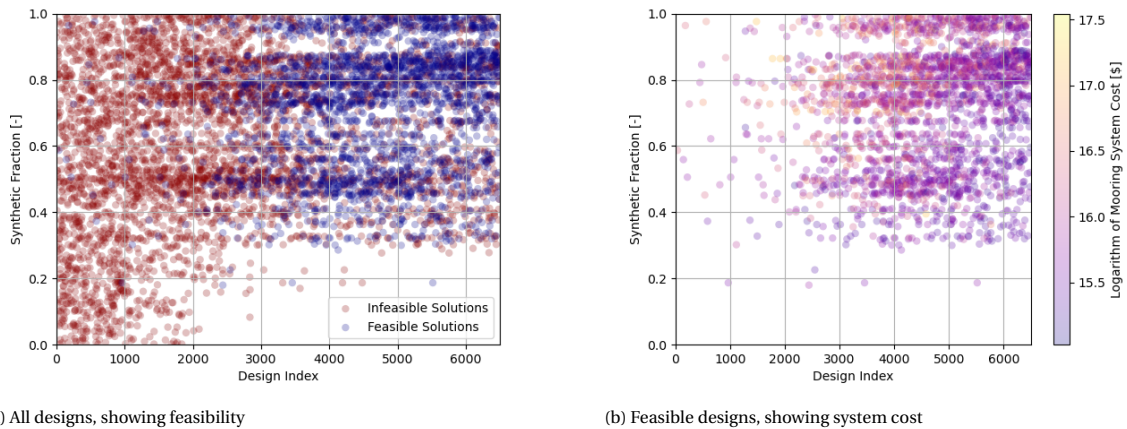


Figure 3.11: Progression of Synthetic Fraction

For the synthetic fraction, as presented in Figure 3.11, another clear reduction of the design space occurs. Here, no feasible results are found with a fraction of the line being composed of synthetic material below about 0.2, while the feasibility rate only significantly increases above 0.3. The feasibility rate is clearly the highest above 0.7, as shown in Figure 3.12, with a 0.46 feasibility rate in total and 0.73 in the final 25 generations. This is quite interesting, as one would assume that the violation of the constraint on the depth of the connection between synthetic and chain lines would be violated more often for designs with a large fraction of the mooring line length being synthetic. Further, the stiffness and minimum breaking load of the polyester line are lower at every diameter and the maximum diameter of the synthetic lines is also lower than for the chain lines, with any chain line with a diameter of at least 0.197 m will have a greater stiffness and minimum breaking load than any possible synthetic line. However, it is unsurprising that much of the designs that are evaluated are concentrated here, as synthetic line is about an order of magnitude cheaper per unit length for the same diameter. Perhaps it is simply this higher diversity of designs evaluated that causes the increased rate of feasibility, with 58% of designs over the last 25 generations having a synthetic fraction of greater 0.7. From Figure 3.11b, it can be seen that initially many of the low cost designs were in fact with a low synthetic fraction, suggesting that design compromises, such as potentially higher mooring line diameters, were necessary to make the highly synthetic systems feasible. However, as the optimisation progressed, significant cost

savings for the highly synthetic designs were achieved, much more than for designs with a lower synthetic fraction, leading to them dominating the final generations.

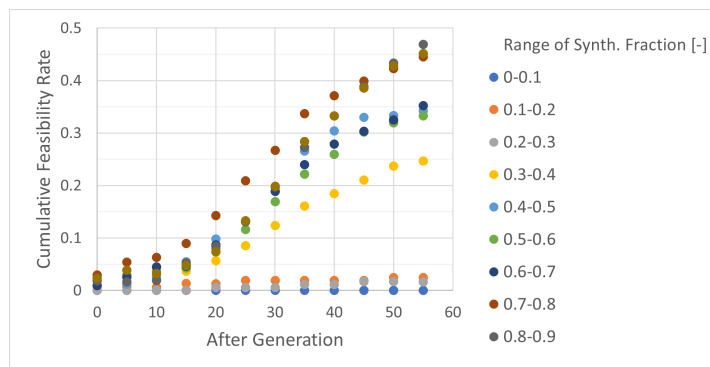
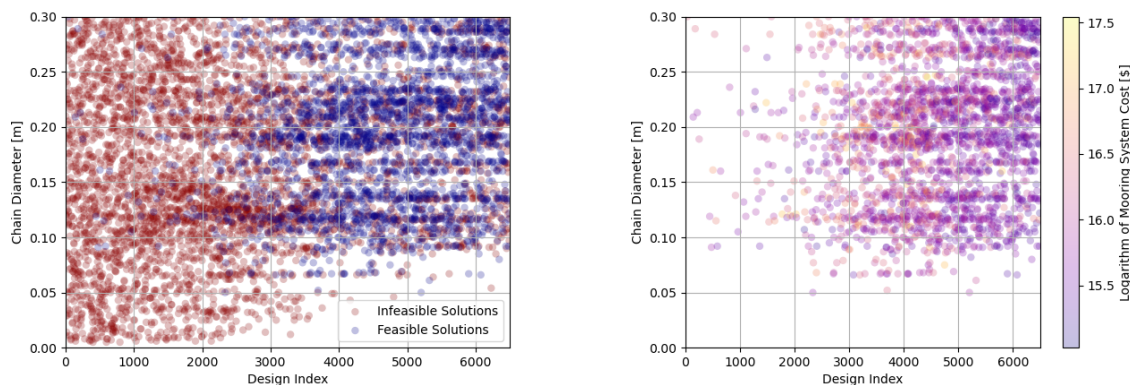


Figure 3.12: Progression of the cumulative feasibility rate for different ranges of synthetic fraction



(a) All designs, showing feasibility

(b) Feasible designs, showing system cost

Figure 3.13: Progression of Chain Line Diameter

The chain line diameter also undergoes a similar restriction of design space to the synthetic diameter, as shown in Figure 3.13a. No feasible designs are found with a chain line diameter below 0.05 m, with the domain generally restricted to around 0.1 m and higher. This is as expected, as the thinner lines simply will not be able to maintain the tension levels required. There is some bias towards higher rates of feasibility for higher diameters, as one would expect, however, it is not so strong. This is because any design with a low chain diameter that is feasible will be low cost, as shown especially in the earlier designs in Figure 3.13b, while for a design with high chain diameter, other elements must be designed more marginally to produce a low cost design. Another factor is the high synthetic fractions, meaning that although the increase of diameter of the chain line incurs a steeper penalty in cost per unit length than for the synthetic lines, this is somewhat offset by the length of the synthetic lines simply being significantly longer.

The synthetic line diameter, meanwhile, clearly shows a strong bias towards a single optimum, as presented in Figure 3.14. Below about 0.075 m, there are almost no feasible designs found, for the same reasons as with the chain line diameter, but above this limit the cost of the mooring system increases rapidly. This is because, like with the chain line, the cost per unit length of the synthetic line increases with the square of the diameter. However, as the large majority of the mooring line length is comprised of synthetic material in most designs, this is a very strong driver of cost savings overall.

Taking a more global overview of the progression, the objective functions of the non-dominated solutions and all feasible solutions can be seen in Figure 3.15a and Figure 3.15b respectively. After 1000 randomly generated solutions, the number of feasible solutions is quite limited, with all solutions falling between \$5 and 20 million. There is a significant range in the anchor radius of the feasible solutions found, between just

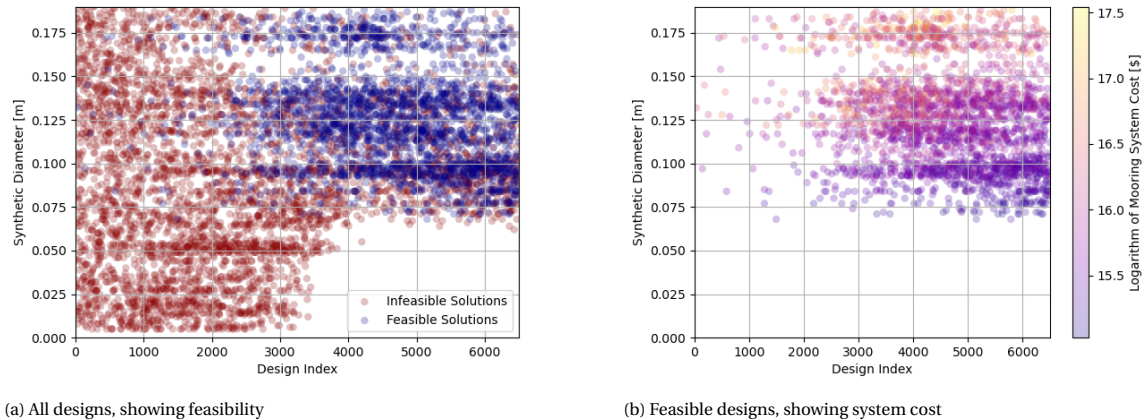


Figure 3.14: Progression of Synthetic Line Diameter

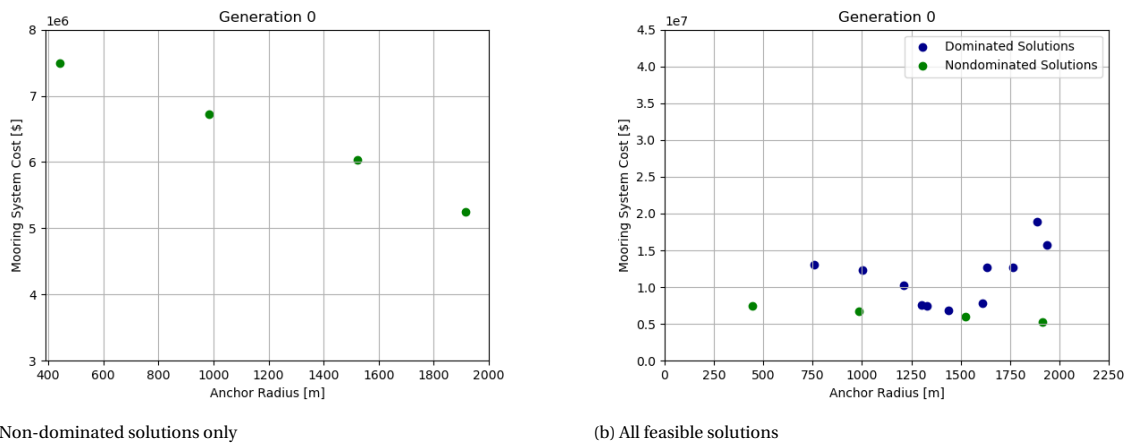


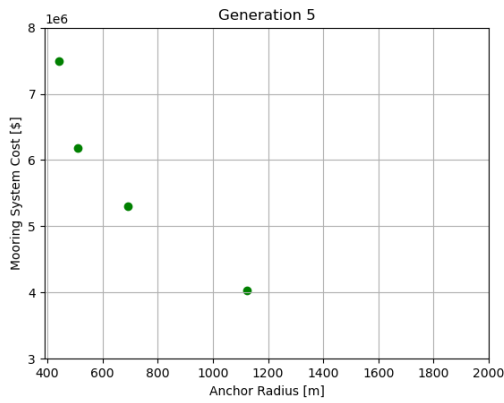
Figure 3.15: Objective functions of solutions after generation 0

over 400 and just under 2000 m. The Pareto front at this point forms a nearly linear progression of 4 of the 16 solutions. Notably, all these solutions are already below \$8 million in cost, which is similar to the most expensive Pareto-optimal solutions at the end of the optimisation.

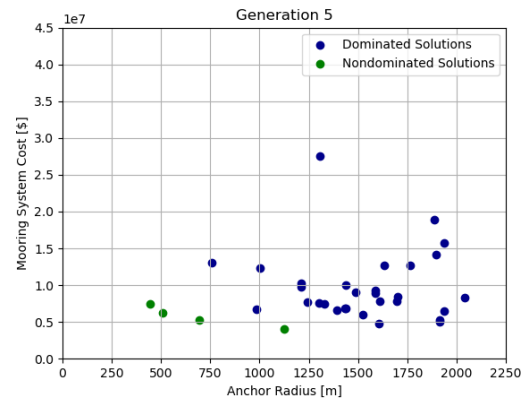
However, there is still a quick progression of the Pareto front. Just 5 generations into the optimisation, there are a significant amount of feasible solutions that have been added, as shown in Figure 3.16b. While most of these new feasible solutions have high anchor radii, it is 3 medium to low radii solutions which are part of the new Pareto front, shown in Figure 3.16a. As mentioned previously, this is in line with predictions, as while it is easier to design a high radius design which is feasible, any low radius designs that do end up being feasible have a good chance to be low cost due simply to the shorter mooring lines. Thus, the new Pareto front is restricted to designs with a radius below 1200 m.

At the approximate halfway mark of the optimisation, after generation 25, the Pareto front has added many more solutions, especially at radii of around 500-600 m, as shown in Figure 3.17a. At this point, the shape of the Pareto front stops being linear and becomes more similar to a rational function. Many more feasible solutions have been found, documented in Figure 3.17b, but many of these are much more expensive and with much higher radii than the Pareto optimal solutions after generation 5, exemplified by the fact that 3 out of the 4 non-dominated solutions after generation 5 have not been dominated in the preceding 20 generations and are still part of the Pareto front.

However, from this point until the termination of the optimisation process after 55 generations, shown in Figure 3.18, significant progress is made. At the lowest cost end of the Pareto front, a reduction in cost of about \$500000 is made in combination with a reduction in radius of about 800 m. Meanwhile, on the lowest

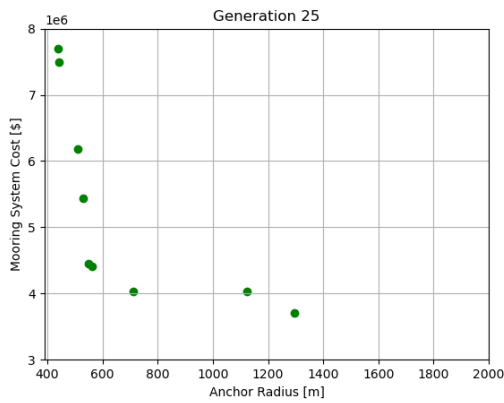


(a) Non-dominated solutions only

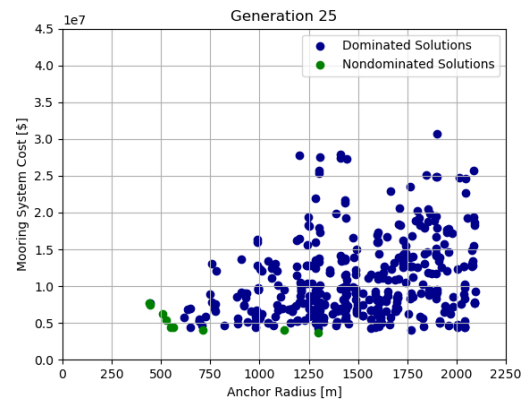


(b) All feasible solutions

Figure 3.16: Objective functions of solutions after generation 5



(a) Non-dominated solutions only



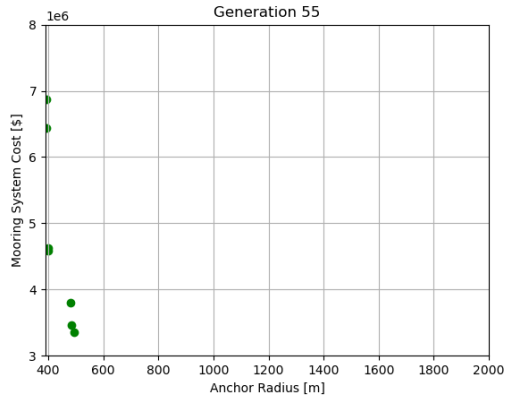
(b) All feasible solutions

Figure 3.17: Objective functions of solutions after generation 25

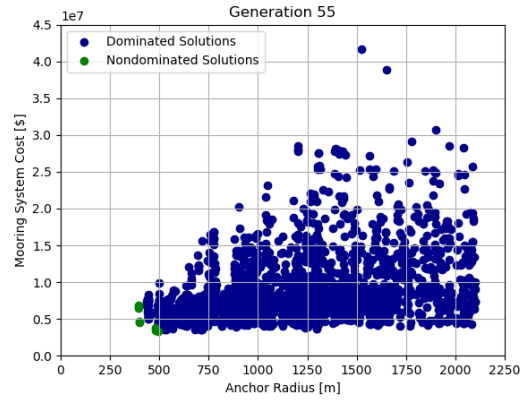
radius end of the Pareto front, a 30 m reduction in radius is achieved along with a reduction in cost of almost \$800000. Furthermore, many more feasible results with anchor radii below 1000 m and/or system costs below \$10 million are found, although most of them are not Pareto-optimal, they provided strong alternative parent options to find better new solutions.

Finally, the constraint violations should be discussed. Of the 12 constraints, there are some which are never violated. The eigenvalues of the system were always positive and the maximum limits on pitch angle, surge eigenfrequency, and tower-base moment were never exceeded. Furthermore, the horizontal excursion limit was not exceeded in the static analysis while the connection depth limit was not exceeded in the extreme load case analyses. However, this does not necessarily mean these constraints are redundant. As mentioned previously, for the load case analysis, connection depth for extreme load cases was a constraint that was violated a number of times, for example. Thus, it can be concluded that due to the random initiation of the population and the large size of the design space, different constraints can be more or less important for the part of the design space from which the optimisation begins. For the remaining constraints, the rates at which they were violated throughout the optimisation are shown in Figure 3.19. These violation rates are relative to the number of times the constraint is evaluated, meaning that if a constraint in a previous tier was violated for a design, this design is counted as neither a pass nor a violation for the later constraints.

As previously discussed, the feasibility rate is below 0.3 until around generation 20, and does not reach 0.7 until generation 30. Thus it is no surprise that the highest violation rates of individual constraints are also seen in the first few generations. Furthermore, as expected, the highest constraint violation rates occur for constraints in the first two tiers, being the constraints on mooring line length, static depth of the synthetic-chain

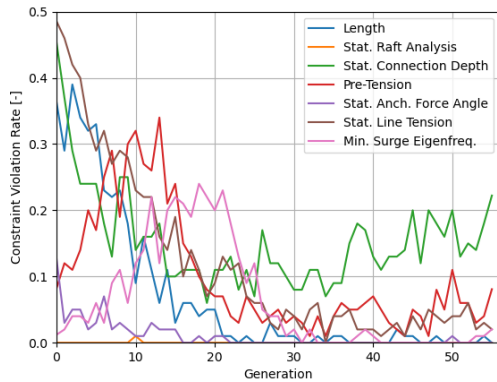


(a) Non-dominated solutions only

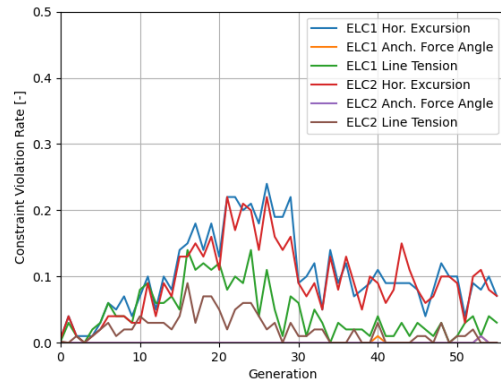


(b) All feasible solutions

Figure 3.18: Objective functions of solutions after generation 55



(a) Geometric, static, and eigenfrequency constraints



(b) Extreme load case constraints

Figure 3.19: Progression of constraint violation rates per generation

line connection, and static mooring line tension. This is indeed a very desirable characteristic, as it means that especially early on when computationally expensive simulations are run, they have a high success rate. Due to the increased penalties for violating these early constraints, however, the population is quickly biased towards designs that do make it through to later tiers of constraints. As the first three constraints quickly reduce, from violation rates between 0.3 and 0.5 to less than 0.2, the also second tiered pre-tension constraint becomes more limiting, followed by the minimum surge eigenfrequency constraint, which is the only constraint that is violated in the third constraint. Again this is positive, with the progression from violation of first tier to second tier to third tier constraints being exactly as the tier system is envisioned to perform optimally.

Alongside the increase in violations of the minimum surge eigenfrequency constraint, there is also an increase in the violations of the extreme load case constraints. After the initial restriction of the design space, these become some of the most critical constraints. Again, this is as the tiered constraint system should work, as it means that the preliminary tiers, many of the constraints in which are simply used to predict violations for the extreme load case constraints, are not too strict as to commonly induce violations in designs which would have passed the extreme load case constraints. The only exception to this is perhaps the static connection depth constraint. This constraint is by a significant margin the most critical constraint towards the end of the optimisation, while the extreme load case connection depth constraints are never violated. This is largely because the extreme load case connection depths are not computed as the maximum of Fourier series, but only as the mean position under loading, as RAFT does not support the tracking of the motion of such extra points. Thus, in fact this is nothing more than extra static analyses, and thus less likely to produce more violations.

It is clear that, of the extreme load case constraints, the horizontal excursions are the most critical, with the line tension constraint seeing more violations early on, but having low importance towards the end of the optimisation. The constraints on the angle of force applied at the anchor are violated only once or twice. The horizontal excursion constraints of the two load cases are violated at very similar rate, though it is still clear that there are a significant number of designs that violate one but not both, as there are disparities. For mooring line tension, however, there are significantly more constraint violations for load case 1 than 2, with no generation seeing a reversal of that trend. This is consistent with the findings in subsection 3.1.1, where load case 1 had mostly line tension constraint violations, which were not present in load case 2 for any designs which did not produce violations for load case 1, while horizontal excursion constraint violations did appear in this sample.

For the earlier tiers of constraints, it is further notable that the pre-tension constraint and the static line tension constraint continue to have a small but significant number of violations until the end of the optimisation. For the pre-tension, this is very much expected, as there is no other constraint that fulfills the same function and the increase of synthetic fraction will cause violations of this constraint. This is also likely the reason for the lack of extreme load case connection depth constraint violations, as the limit to the synthetic fraction is maintained by the pre-tension constraint. This is because the tension in a mooring line is always largest at the fairlead, and lowest at the anchor [31]. Thus, the larger the synthetic fraction, the lower the tension in the synthetic line at the bottom end. The presence of static line tension constraint violations is explained by the tendency of the optimisation to reduce the synthetic line diameter as much as possible, with a significant amount of infeasible designs in later generations having a synthetic line diameter around 0.075 m. Finally, RAFT encounters an error in its static analysis only once during the optimisation, and the static evaluation of the angle of force at the anchor, the minimum force eigenfrequency constraint, and the mooring line length constraint produce only sporadic violations in the later generations, as expected.

3.1.3. Final Results

When inspecting the final results of the mooring system design optimisation, many of the patterns observed during the progression reach their logical conclusion. In Figure 3.20a, the final Pareto front is shown. It is at first notable that the Pareto front spans only a small fraction of the anchor radius domain, with the lowest cost solution having an anchor radius only 100 m larger than the feasible solution with the smallest radius. As can be seen in Figure 3.20b, few of the dominated solutions come close to matching this system cost, with only a few solutions with an anchor radius above 750 m having costs just below \$4,000,000. While there are a significant amount of solutions with high anchor radii that have lower costs than at least one of the Pareto-optimal solutions, it is also clear that there are significantly more feasible solutions with lower anchor radii, particularly in the 500 to 1000 m range. However even this range of radii does not produce a Pareto-optimal solution. In previous research [45], [46], it was also found that the maximum anchor radius at which cost improvements could be found was quite low, with the studies finding a maximum Pareto-optimal anchor radius of about 265 and 400 m respectively for water depths of 55 and 56 m. Thus, in combination with the minimum anchor radii found in those studies that were mentioned earlier, this seems to confirm that the limited range of anchor radii found is a valid result. The latter study also finds mooring system costs of between \$1.2 and 1.5 million for the same floater and turbine combination, however, which is significantly lower than what is found in this research. The main reason for this seems to be that the study by West does not use any safety factors excluding a fatigue factor, while in this research on top of a corrosion and wear factor extra safety factors are used as recommended in relevant standards [25], [50], [56], [57]. These include safety factors of 1.5 on the maximum anchor loading and 2.0 on the mooring tension. In combination with the higher water depths and slightly more extreme metocean conditions, this should explain the differences in cost.

When looking in particular at the design variables for the final Pareto-optimal solutions in Table 3.4, it is clear that the designs are fairly similar. The difference between the maximum and minimum of each design variable used is just 100 m for the anchor radius, and 0.047 m for the synthetic line diameter. However, there are slightly larger differences for the line length ratio (0.043), synthetic fraction (0.145) and chain line diameter (0.100 m). The only correlation between design variables that is of note is between line length ratio and anchor radius, but even this is far short of statistical significance.

However, there are trends in where in the design space the Pareto-optimal solutions fall. For the line length ratio, it is in fact notable that the designs represent a large segment of the range in which feasible solutions

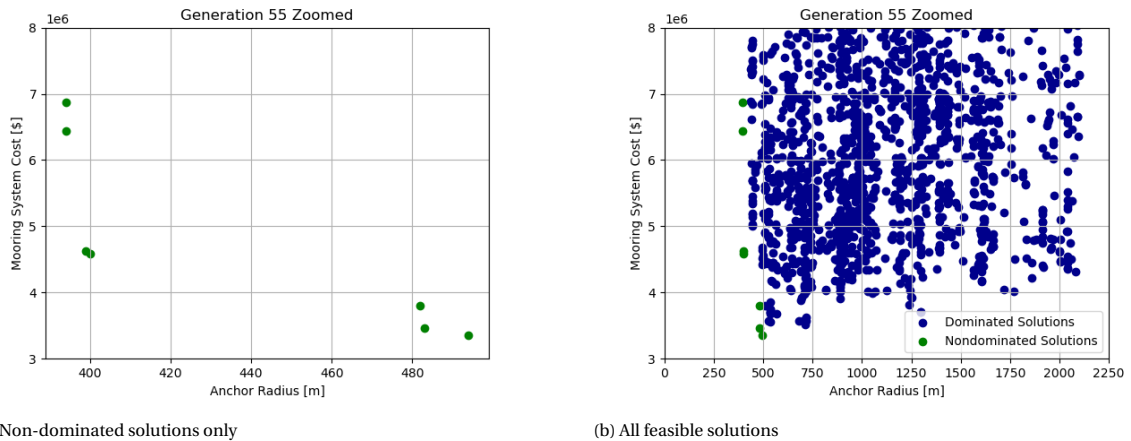


Figure 3.20: Objective functions of solutions at the conclusion of the optimisation, with focus on the well-performing solutions

were found, as this was limited, with very few and costly exceptions, to between 0.94 and 1.02, with the range of Pareto-optimal solutions covering more than half of this feasible range. This is in line with the earlier assertion that the line length ratio does not have a very significant impact on the mooring system cost.

For the synthetic fraction, the Pareto optimal solutions are all towards the upper part of the feasible range in the design space, though it is notable that only one Pareto-optimal surpasses a synthetic fraction of 0.9. As mentioned, the synthetic lines are much cheaper per unit length than the chain lines, thus this is to be expected.

Further, all Pareto-optimal solutions have synthetic line diameters close to the minimum that was found to be feasible in the optimisation, which is especially important to reduce costs due to the very high synthetic fraction. Finally, the chain line diameters seen in the final results sit in the middle third of the feasible range for the variable, once again confirming the lack of a strong correlation between the chain line diameter and system cost due to the high synthetic fraction.

Table 3.4: Design variables and cost of solutions on the final Pareto front

Line Length Ratio [-]	1.005	0.994	1.014	0.973	0.971	0.971
Synthetic Fraction [-]	0.816	0.819	0.796	0.941	0.854	0.878
Anchor Radius [m]	394	399	400	482	483	494
Synthetic Line Diameter [m]	0.119	0.104	0.088	0.085	0.072	0.072
Chain Line Diameter [m]	0.257	0.279	0.157	0.220	0.201	0.201
Mooring System Cost [M\$]	6.441	4.625	4.582	3.807	3.458	3.352

3.2. Layout and Cable Routing Optimisation

In the layout and cable routing optimisation, the placement of the turbines, selection of the mooring system from the Pareto-optimal solutions presented above, and its orientation, and the routing of cables between turbines and from turbines to substations is determined with the objective to maximise the NPV of the project. In the following sections, the individual layouts is discussed in subsection 3.2.1, and the overall influence of different factors is presented in section 3.3.

3.2.1. Individual layouts

The case study uses an adapted version of instance B from the work of Cazzaro et al. [54], with a constant water depth and an added clearance zone around substations, referred to as the safety zone in the rest of this thesis. The instance includes irregular boundaries, fixed substation points, obstacles within the boundaries, and an adjacent wind farm which influences the power production of turbines in this wind farm. Performing

the bottom-fixed wind farm layout optimization with the added safety radius produces the turbine placements shown in Figure 3.21. From the placement of the turbines, it can be inferred that the wind primarily blows from the west and southwest directions, as the turbines are mostly placed in banks perpendicular to this direction. Consulting the wind rose in Figure 3.22 confirms that this is indeed the case. The effects of the cable routing portion of the optimisation are clear, as the turbines are largely placed in distinct rows, barely further apart than the minimum distance requirement mandates. For some of the rows, there is a significant distance to the substation, such as the turbines placed in the northwest of the zone. In terms of its structure, this layout is visually similar to the layout from the work of Cazzaro [16] shown in Figure 2.2.

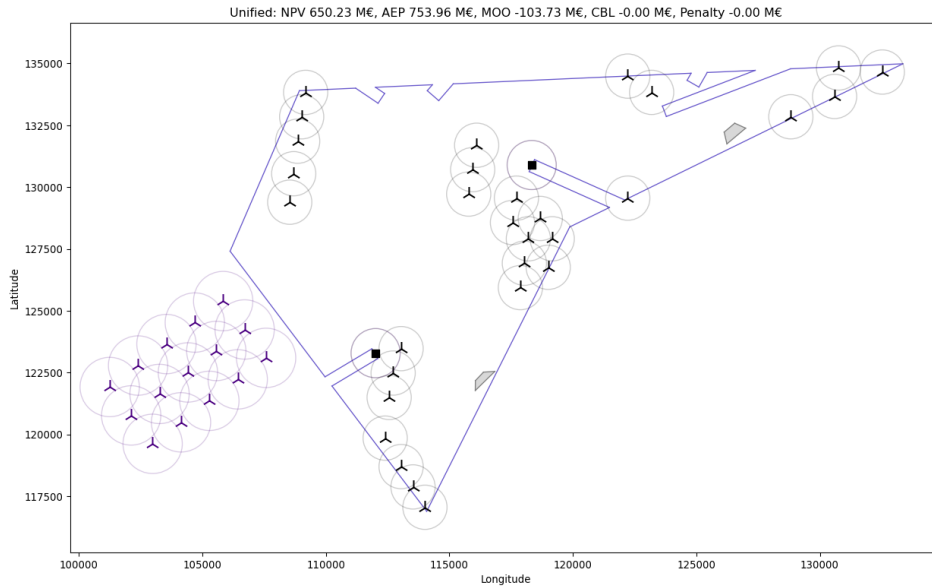


Figure 3.21: Placement of 30 turbines on wind farm instance B from the CWFOP with safety radius

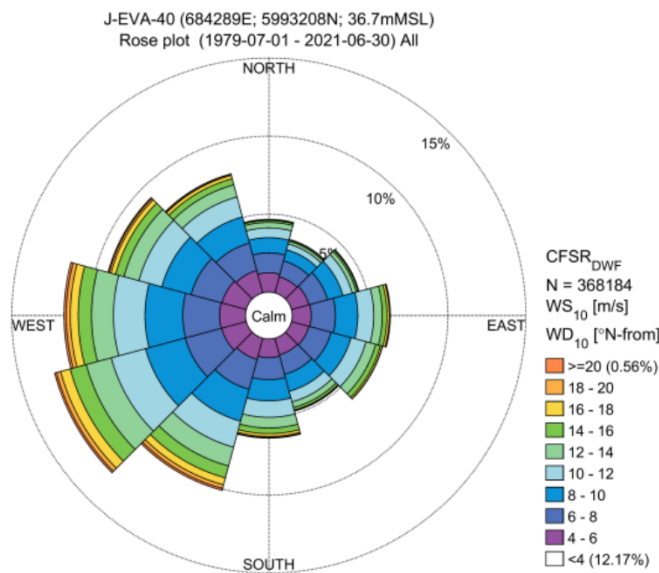


Figure 3.22: Wind Rose for the Ten Noorden van de Waddeneilanden wind farm zone [55]

The first mooring system which was tested was the smallest system with an anchor radius of 394 m. It was initialised with an orientation offset of 0°, meaning that the centre line of one of the legs faced directly due North. The result of this optimisation can be seen in Figure 3.23. As one can see, the combination of this orientation and the placement of the turbines due to the prevalent wind direction means that there are many

anchors nearly directly in the straight line path between two adjacent turbines, meaning that the cables must take a longer route to avoid the anchors. This also becomes a concern near the substation, where multiple strings of turbines must be connected. As can be seen with the Southwestern substation, the mooring systems of turbines in proximity to the substation can require significant deviations from the cable routing for strings that do not include those turbines. This is the main reason for the incorporation of the safety radius. As can be seen, two turbines are placed exactly on the edge of the safety radius of the Southwestern substation, as close proximity to the substation provides obvious cable routing benefits when mooring systems are not a concern. However, because cables are prohibited from crossing mooring lines or from routing within 100 m of anchors, turbines that are very close to the substation will block access to it for any string that does not connect to the substation through those turbines.

Immediately from this first layout, some limitations of the process become clear. Firstly, the layout optimization program does not have the capacity to rotate a mooring system in its entirety. It can adjust individual anchors within specified tolerances to avoid obstacles, but these must be kept small to maintain the overall design of the system. This adjustment can be seen with the turbines in the Northeastern corner, who's anchors on the Southwestern leg are adjusted to be slightly more due West. However, due to the lack of a unified rotation mechanism and that this can only be used for obstacles and the farm boundary, it is often not possible to fully resolve the clashes with obstacles and the windfarm boundary, and it isn't possible to use the rotation of individual mooring systems to improve the cable routing.

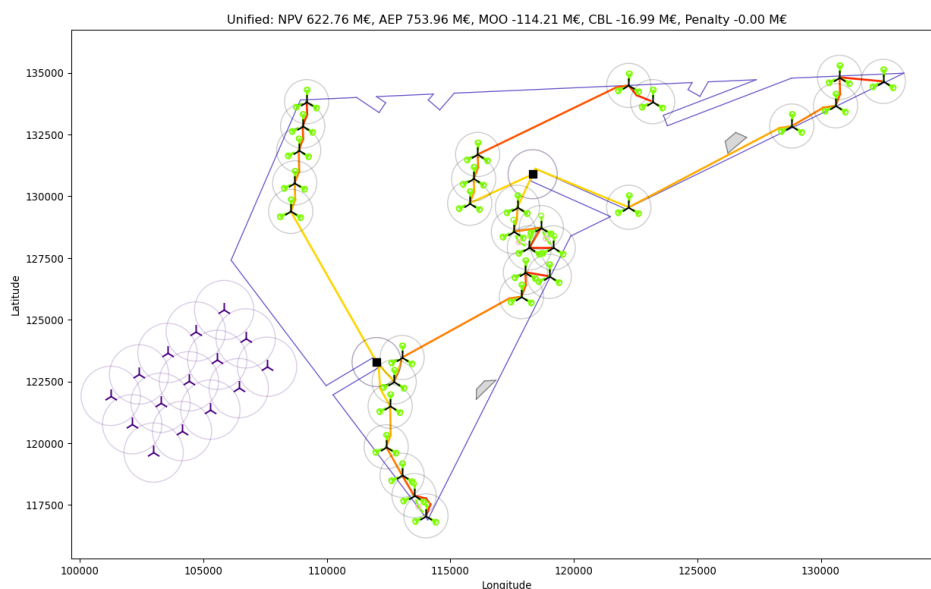


Figure 3.23: Optimal layout with the mooring system with an anchor radius of 394 m at a 0° offset with 30 turbines

When comparing the cable routing discussed above to the cable routing for a case where the same mooring system is rotated by 40° clockwise for every turbine, it is notable that there are few differences. The order in which turbines are connected is only different in one string, which is the penultimate and third last turbines on the string which extends to the South of the Northeastern substation, which are swapped. It is thus unsurprising that the cable routing costs only change slightly, decreasing by 20000€, or 1.2%. As the cable routing is the smallest contribution to the NPV, and as the turbine placements and mooring system used do not change, the increase in NPV is only 0.03%. An offset of 80° was also used, as shown in Figure 3.25. Between this layout and the layout with an offset of 40°, there are no differences in which turbines are connected, but some slightly longer cable routes mean that the cable cost increases by 70000€, or 0.4%.

When comparing the layouts using the two largest mooring systems, shown in Figure 3.26 and Figure 3.27, one can see that in fact there is no difference at all with the cable routing from Figure 3.24. Thus, the reductions achieved by using a cheaper mooring system do not incur any penalty in increased cable costs. This indicates that, at least in a fairly sparse wind farm such as the case with 30 turbines, there is no advantage to a joint optimisation of mooring system and layout, as using the mooring system with the lowest cost does not produce any cost increases in other systems.

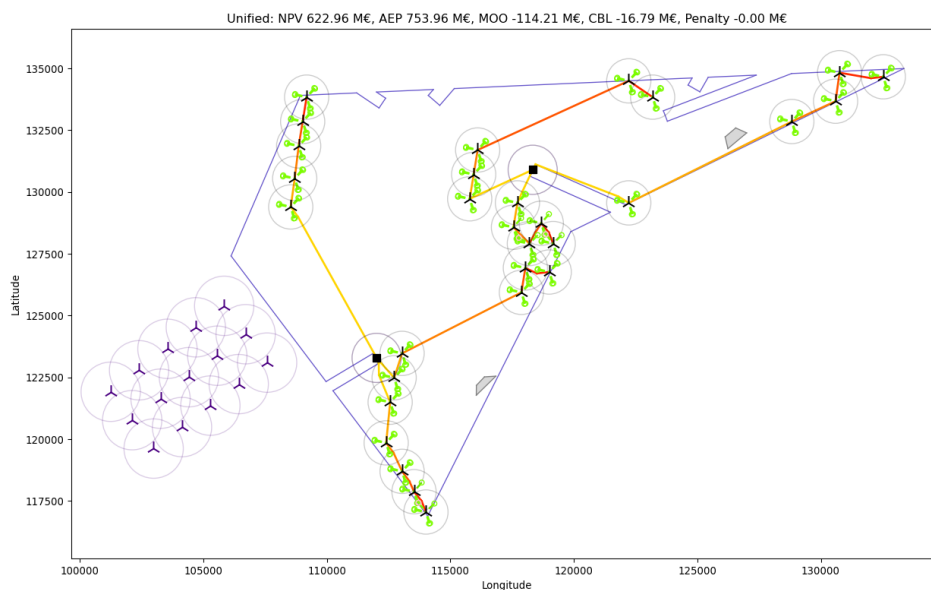


Figure 3.24: Optimal layout with the mooring system with an anchor radius of 394 m at a 40° offset with 30 turbines

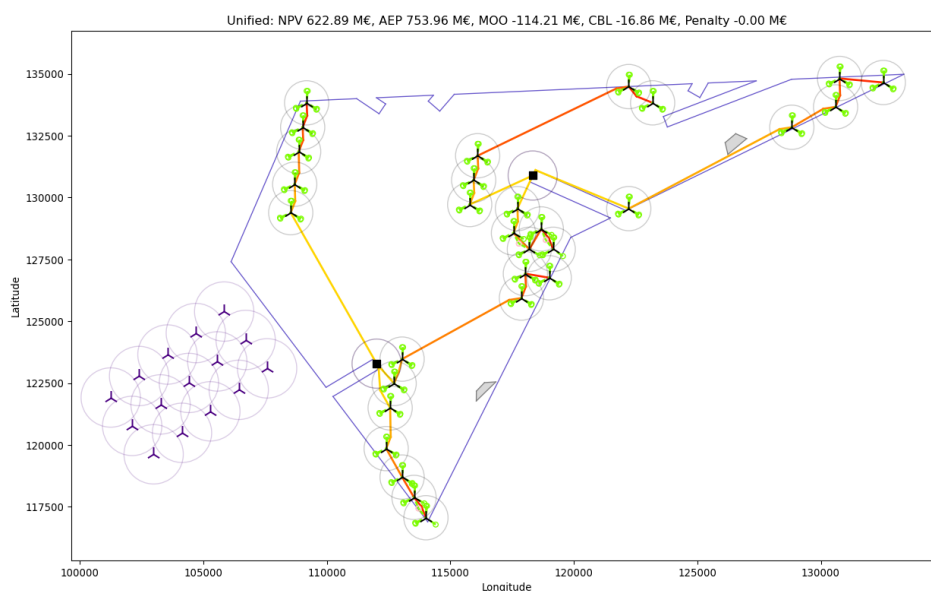


Figure 3.25: Optimal layout with the mooring system with an anchor radius of 394 m at a 80° offset with 30 turbines

It was attempted to compare the findings from the 30 turbine farm with a more dense farm. In theory, one would expect that at a high enough density, using a mooring system with a smaller footprint would have an advantage. Thus, a layout for 60 turbines was created, which is shown in Figure 3.28. However, when attempts were made to introduce mooring systems to this layout, it was not possible to find a feasible cable routing solution for any mooring system in any of the three orientations used. To explore the limitations, the final attempt for the cable routing produced by the optimization process is shown in Figure 3.29. As can be seen, the two most Northwestern strings from the Western substation have crossing cables, as do the two most Western strings from the Eastern substation. The Southeastern string from the Eastern substation crosses itself, while the Western branch from the Western substation passes through the location of the substation from Southwest to Northwest before making a small loop to incorporate the final 3 turbines. The reason for the issues with finding a feasible cable routing are clear, the turbines are simply too close together, creating a chain of mooring systems which block any cables from passing between them. The cable routing is not able to find a detour around these blocks, leading to an infeasible result. In order to be able to find feasible results

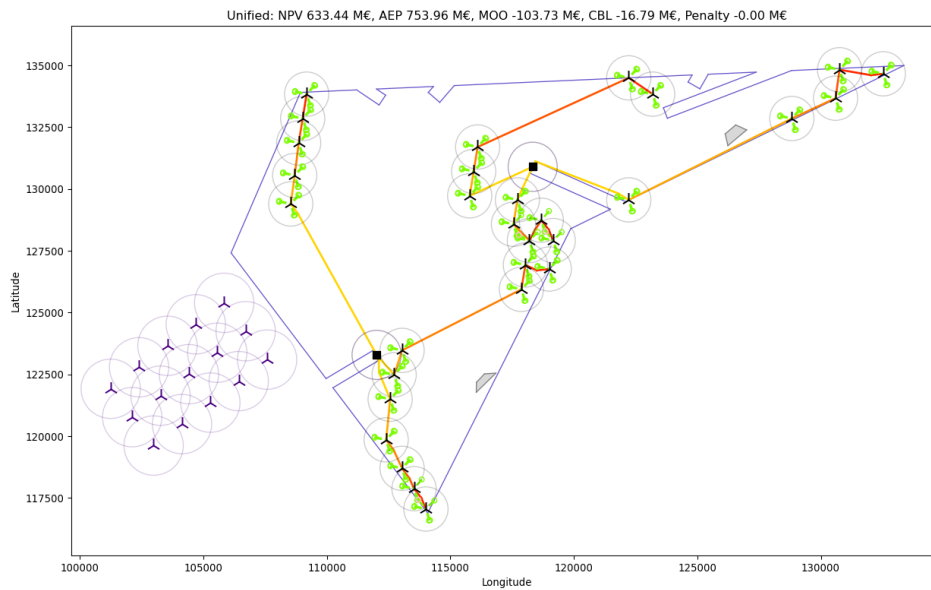


Figure 3.26: Optimal layout with the mooring system with an anchor radius of 483 m at a 40° offset with 30 turbines

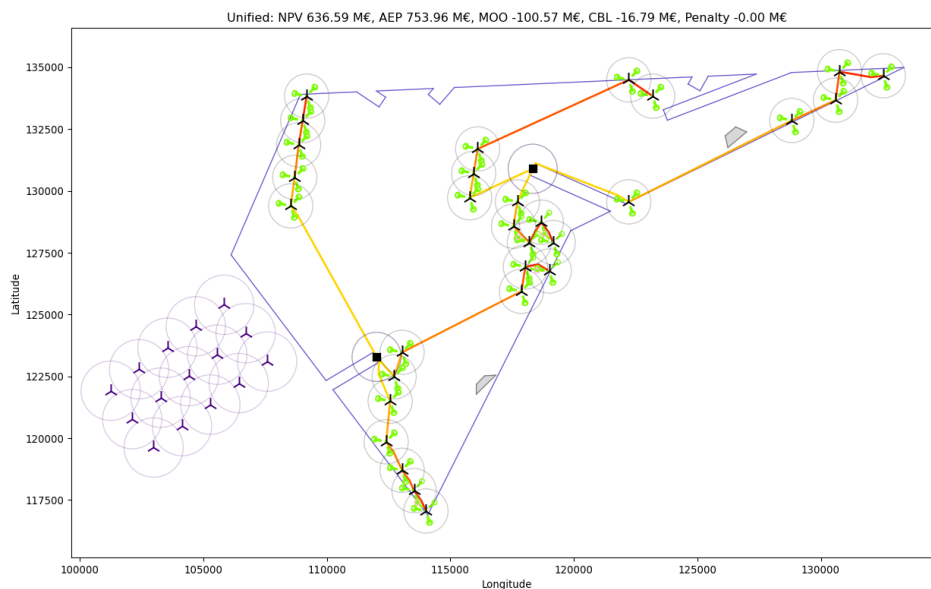


Figure 3.27: Optimal layout with the mooring system with an anchor radius of 494 m at a 40° offset with 30 turbines

in more dense wind farms, there are numerous changes which have to be implemented.

First, the turbines must have a second minimum distance requirement, both from each other and from the boundary of the wind farm, which is dependent on the mooring system. Unlike with the regular turbine minimum distance requirement, this minimum distance requirement should not overlap with the minimum distance requirements of other turbines, rather than only the turbine itself not overlapping. Second, full rotation capabilities of individual mooring systems are necessary, in order to avoid obstacles and farm boundaries, and to allow an adjustment to open a path between two mooring systems for cables to go. Third, the cable routing optimization should be adjusted such that it is more easily able to find a different way to connect up a turbine if the optimal connection without mooring system interference is not reachable.

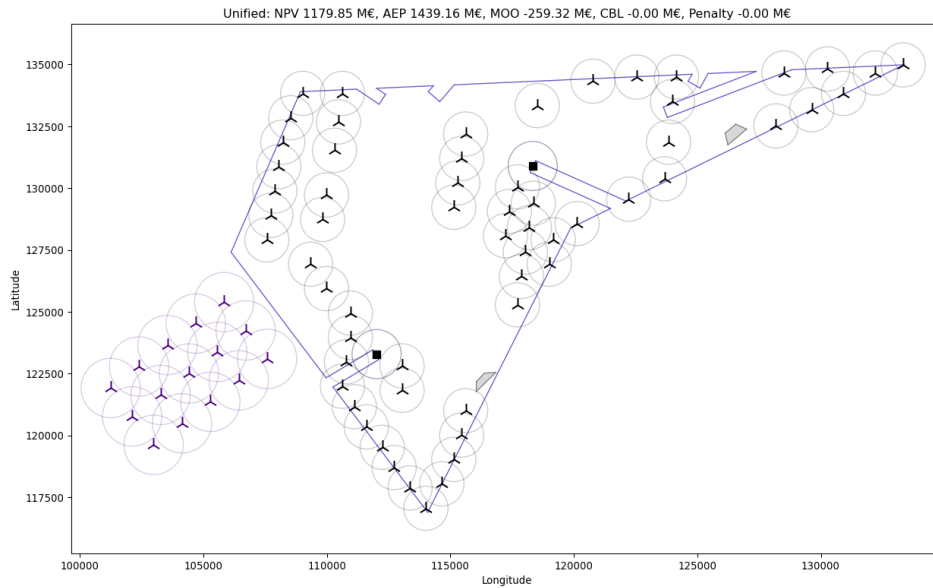


Figure 3.28: Placement of 60 turbines on wind farm instance B from the CWFOP with safety radius

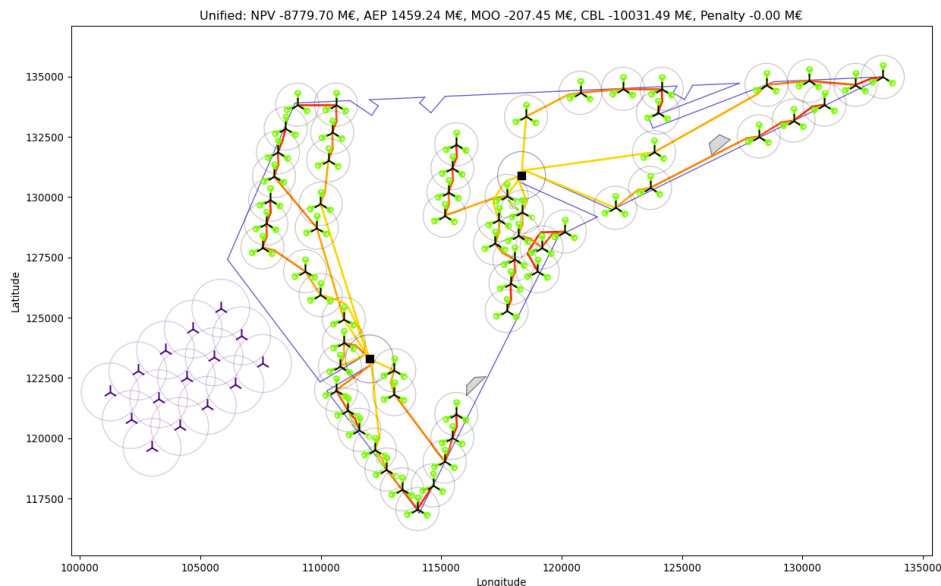


Figure 3.29: Final layout found in optimization for the mooring system with an anchor radius of 483 m at a 0° offset with 60 turbines

3.3. Optimization and Parameter Study

As mentioned, the advantages to using a cheaper but larger mooring system are not counterbalanced by any disadvantages. This is further illustrated in Figure 3.30 and Figure 3.31. There is a clear directly linear relationship between mooring costs and NPV, meaning that there does not seem to be any law of diminishing returns where eventually an optimum would be reached and further decreasing the costs of the mooring system would decrease the overall NPV. The only limiting factor is the optimum in the cost of the mooring system itself, which as seen before does not decrease further with increased mooring radius beyond a certain point.

Another crucial point is that the mooring costs for a wind farm and the inter-array cable costs are of different orders of magnitude, which means that a 1% decrease in mooring costs would lead to increased NPV even if the cable costs would increase by nearly 10%. Finally, as shown in Figure 3.32, there is indeed a difference depending on the orientation of the mooring systems for the cable costs. However, the potential

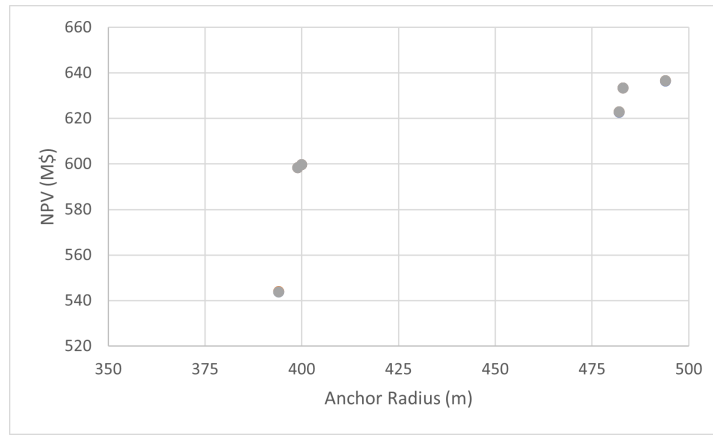


Figure 3.30: Relationship between the anchor radius of the mooring system with 40° offset and the NPV of a 30 turbine wind farm

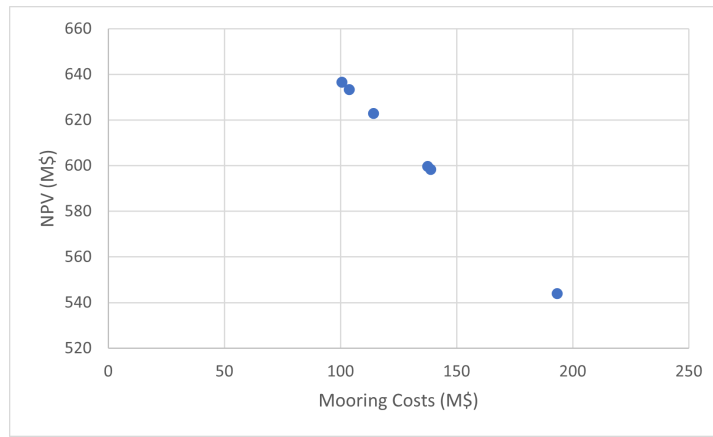


Figure 3.31: Relationship between the costs of the mooring system with 40° offset and the NPV of a 30 turbine wind farm

savings are very slight if the orientation of all mooring systems is kept the same.

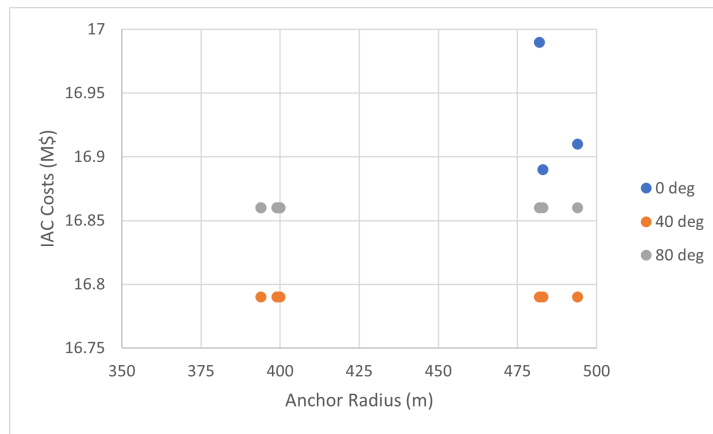


Figure 3.32: Relationship between the anchor radius of the mooring system with all offsets and the inter-array cable costs of a 30 turbine wind farm

4

Conclusions and Recommendations

Before concluding, it is useful to restate the objective of this thesis. The objective of this thesis was to understand the benefits of integrating mooring design into the wind farm layout optimisation process and finding an implementation for this. In order to do so, it was investigated which mooring models are suited to use in optimisation, at what stage of the wind farm layout optimisation process the mooring system design can be best implemented, what the couplings are between mooring design, turbine placement, and cable routing to produce an improved wind farm design, and to what extent the integrated approach improves the design of the wind farm.

The investigation into mooring models led quickly to the conclusion that a frequency-domain model was necessary, due to the number of simulations and evaluations that are necessary in an optimisation context. As the mooring system and therefore the system properties are constantly changing, even models which only use time domain simulations for pre-processing are unsuitable. Therefore, it was chosen to use the software RAFT developed by Hall et al [42].

Mooring system design is largely independent from the turbine placement or cable routing in a wind farm, assuming the changes in water depth are not significant. However, the turbine placement for an effective or even a feasible windfarm layout is heavily dependent on the mooring system design. Thus, the mooring system design should be performed before the turbine placement, such that the results can be used to inform the spacing between turbines and from turbines to the boundary of the wind farm.

Mooring design does not have a significant impact on the cable routing in terms of costs, per the current methods. However, mooring systems can cause it to be impossible to find a feasible cable routing. Furthermore, as mentioned, turbines require different spacing depending on the anchor radius of a mooring system.

With the current methods, the implementation of an integrated optimisation and design approach, whereby multiple mooring systems with different characteristics are used to design the best overall floating wind farm has no benefits over simply designing a single mooring system and then designing a wind farm for this specific mooring system. This is because the best mooring system for a single turbine provides such significant cost savings that using a mooring system which is more expensive but has a smaller footprint does not provide any gains.

For further research, it is recommended to first take a step back and further investigate the methods for wind farm layout design for floating wind farms, as the current methods have been found to be lacking. Only once these methods have been sufficiently improved would it be worthwhile to revisit the question of mooring design and its place within the larger floating wind farm design process.

In conclusion, with the current state of floating wind farm layout optimisation and design processes, the integration of mooring design does not bring any benefits, and while implementation is possible, further work needs to be done on floating wind farm layout optimisation itself first.

Bibliography

- [1] {Vattenfall}, *Vattenfall gives go-ahead for Kriegers Flak offshore wind farm*, Dec. 2018.
- [2] K. Calvin, D. Dasgupta, G. Krinner, *et al.*, “IPCC, 2023: Climate Change 2023: Synthesis Report. Contribution of Working Groups I, II and III to the Sixth Assessment Report of the Intergovernmental Panel on Climate Change [Core Writing Team, H. Lee and J. Romero (eds.)]. IPCC, Geneva, Switzerland,,” Intergovernmental Panel on Climate Change, Tech. Rep., Jul. 2023. DOI: 10.59327/IPCC/AR6-9789291691647. [Online]. Available: <https://www.ipcc.ch/report/ar6/syr/>.
- [3] International Energy Agency, “Net Zero by 2050 - A Roadmap for the Global Energy Sector,” Tech. Rep., 2050. [Online]. Available: www.iea.org/t&c/.
- [4] “GWEC.NET Associate Sponsors Podcast Sponsor Leading Sponsor Supporting Sponsor Co-leading Sponsor,” Tech. Rep. [Online]. Available: www.gwec.net.
- [5] A. Myhr, C. Bjerkseter, A. Ågotnes, and T. A. Nygaard, “Levelised cost of energy for offshore floating wind turbines in a lifecycle perspective,” *Renewable Energy*, vol. 66, pp. 714–728, 2014, ISSN: 09601481. DOI: 10.1016/j.renene.2014.01.017.
- [6] M Collu, A. J. Kolios, A Chahardehi, and F Brennan, “A COMPARISON BETWEEN THE PRELIMINARY DESIGN STUDIES OF A FIXED AND A FLOATING SUPPORT STRUCTURE FOR A 5 MW OFFSHORE WIND TURBINE IN THE NORTH SEA,” Tech. Rep.
- [7] M. Hannon, E. Topham, J. Dixon, D. Mcmillan, and M. Collu, “Offshore wind, ready to float? Global and UK trends in the floating offshore wind market,” DOI: 10.17868/69501. [Online]. Available: <https://doi.org/10.17868/69501>.
- [8] A Martinez and G Iglesias, “Mapping of the levelised cost of energy for floating offshore wind in the European Atlantic,” English, *Renewable and Sustainable Energy Reviews*, vol. 154, 2022, ISSN: 13640321 (ISSN). DOI: 10.1016/j.rser.2021.111889. [Online]. Available: <https://www.scopus.com/inward/record.uri?eid=2-s2.0-85118893621&doi=10.1016%2fj.rser.2021.111889&partnerID=40&md5=5b93a2fdbc62ff2dd8f6a6a1d7c7fe2b>.
- [9] M Lerch, M De-Prada-Gil, C Molins, and G Benveniste, “Sensitivity analysis on the levelized cost of energy for floating offshore wind farms,” English, *Sustainable Energy Technologies and Assessments*, vol. 30, pp. 77–90, 2018, ISSN: 22131388 (ISSN). DOI: 10.1016/j.seta.2018.09.005. [Online]. Available: <https://www.scopus.com/inward/record.uri?eid=2-s2.0-85053751309&doi=10.1016%2fj.seta.2018.09.005&partnerID=40&md5=ae0b7b130180ed7b5b3a88b92a222e41>.
- [10] J. M. Hegseth, E. E. Bachynski, and J. R. Martins, “Integrated design optimization of spar floating wind turbines,” *Marine Structures*, vol. 72, Jul. 2020, ISSN: 09518339. DOI: 10.1016/j.marstruc.2020.102771.
- [11] E. Gaertner, J. Rinker, L. Sethuraman, *et al.*, “Definition of the IEA Wind 15-Megawatt Offshore Reference Wind Turbine Technical Report,” Tech. Rep., 2020. [Online]. Available: www.nrel.gov/publications.
- [12] C. Allen, A. Viselli, H. Dagher, *et al.*, “Definition of the UMaine VoltturnUS-S Reference Platform Developed for the IEA Wind 15-Megawatt Offshore Reference Wind Turbine Technical Report,” Tech. Rep., 2020. [Online]. Available: www.nrel.gov/publications.
- [13] Y. Liu, S. Li, Q. Yi, and D. Chen, *Developments in semi-submersible floating foundations supporting wind turbines: A comprehensive review*, Jul. 2016. DOI: 10.1016/j.rser.2016.01.109.
- [14] D. Marten, J. Saverin, R. Behrens de Luna, and S. Perez-Becker, *Validation Tests for Potential Flow Models with Morison Drag (LPMD)*, 2021. [Online]. Available: <https://docs.qblade.org/src/validation/hydrodynamics/lpmd/lpmd.html>.
- [15] A. Tesauro, P.-E. Réthoré, and G. C. Larsen, “State of the art of wind farm optimization,” in *Proceedings of EWEA 2012 - European Wind Energy Conference & Exhibition*, vol. 19, European Wind Energy Association (EWEA), 2012.

- [16] D. Cazzaro, "Unified Optimization for Offshore Wind Farm Design," Ph.D. dissertation, Technical University of Denmark, Kgs. Lyngby, Aug. 2022.
- [17] M. Y. Mahfouz, M. Hall, and P. W. Cheng, "A parametric study of the mooring system design parameters to reduce wake losses in a floating wind farm," in *Journal of Physics: Conference Series*, vol. 2265, Institute of Physics, Jun. 2022. DOI: 10.1088/1742-6596/2265/4/042004.
- [18] M. Y. Mahfouz and P.-W. Cheng, "A passively self-adjusting floating wind farm layout to increase the annual energy production," English, *Wind Energy*, vol. 26, no. 3, pp. 251–265, 2023, ISSN: 10954244 (ISSN). DOI: 10.1002/we.2797. [Online]. Available: <https://www.scopus.com/inward/record.uri?eid=2-s2.0-85143982657&doi=10.1002%2fwe.2797&partnerID=40&md5=7756668e5628e6c81a15a40606c0f2d6>.
- [19] M. Y. Mahfouz and P. W. Cheng, "A passively self-adjusting floating wind farm layout to increase the energy production: A sensitivity analysis," in *Journal of Physics: Conference Series*, vol. 2626, Institute of Physics, 2023. DOI: 10.1088/1742-6596/2626/1/012053.
- [20] M. Y. Mahfouz, E. Lozon, M. Hall, and P. W. Cheng, "Dynamic performance of a passively self-adjusting floating wind farm layout to increase the annual energy production," *Wind Energy Science*, no. preprint, 2023. DOI: 10.5194/wes-2023-135. [Online]. Available: <https://doi.org/10.5194/wes-2023-135>.
- [21] V. Ceriello, "Wake Effect Mitigation of Floating Offshore Wind Farms Combining Layout Optimization, Turbine Repositioning and Yaw-based Wake Redirection Vincenzo Ceriello," Ph.D. dissertation, Delft University of Technology, Delft, NL, Jul. 2023. [Online]. Available: <https://github.com/Vincer99/VCeriello-Thesis-Code>.
- [22] U. Kilinc, "Dynamic wind farm layout optimization," Ph.D. dissertation, Delft University of Technology, Delft, NL, Aug. 2022.
- [23] K.-T. Ma, Y. Luo, T. Kwan, and Y. Wu, "Mooring for floating wind turbines," in *Mooring System Engineering for Offshore Structures*, Elsevier, 2019, pp. 299–315. DOI: 10.1016/b978-0-12-818551-3.00015-6.
- [24] "Wind energy generation systems-Part 3-2: Design requirements for floating offshore wind turbines," International Electrotechnical Commission, Geneva, CH, Tech. Rep., Apr. 2019.
- [25] "Olie-og naturgasindustrien-Specifikke krav til offshorekonstruktioner-Del 7: Stationkeeping-systemer til flydende offshoreanlaeg og mobile offshore-enheder Petroleum and natural gas industries-Specific requirements for offshore structures-Part 7: Stationkeeping systems for floating offshore structures and mobile offshore units," Tech. Rep., 2013.
- [26] R. Yang, X. Zheng, J. Chen, and Y. Wu, "Current Status and Future Trends for Mooring Systems of Floating Offshore Wind Turbines," *Sustainable Marine Structures*, vol. 4, no. 2, Sep. 2022. DOI: 10.36956/sms.v4i2.617.
- [27] T. Fulton, Y. Arikian, R. Miller, J. K. Longridge, and M. Campbell, "Design and Installation of Leading Edge, Practical and Economic Mooring Systems for Commercial Scale Floating Offshore Wind Energy," English, in *Proceedings of the Annual Offshore Technology Conference*, Offshore Technology Conference, 2021, ISBN: 01603663 (ISSN); 978-161399787-1 (ISBN). DOI: 10.4043/31318-MS. [Online]. Available: <https://www.scopus.com/inward/record.uri?eid=2-s2.0-85149297595&doi=10.4043%2f31318-MS&partnerID=40&md5=c1ac37e83512a16e5fc7c05f66a086af>.
- [28] C. H. Kim, C. Zhao, and J. Zou, "Springing and Ringing Due to Nonlinear Waves on a Coupled TLP," in *Proceedings of the Fifth (1995) International Offshore and Polar Engineering Conference*, The Hague, NL: International Society of Offshore and Polar Engineers (ISOPE), Jun. 1995, pp. 83–89, ISBN: 1880653168.
- [29] A. Peccin da Silva, "Anchoring systems for floating wind turbines," May 2023.
- [30] K.-T. Ma, Y. Luo, T. Kwan, and Y. Wu, "Mooring design," in *Mooring System Engineering for Offshore Structures*, Elsevier, 2019, pp. 63–83. DOI: 10.1016/b978-0-12-818551-3.00004-1.
- [31] K.-T. Ma, Y. Luo, T. Kwan, and Y. Wu, "Mooring analysis," in *Mooring System Engineering for Offshore Structures*, Elsevier, 2019, pp. 85–114. DOI: 10.1016/b978-0-12-818551-3.00005-3.
- [32] M. Hall and A. Goupee, "Validation of a lumped-mass mooring line model with DeepCwind semisubmersible model test data," Tech. Rep., 2015.

- [33] M. Hall, "Efficient Modelling of Seabed Friction and Multi-Floater Mooring Systems in MoorDyn," in *12th European Wave and Tidal Energy Conference*, Cork, IE, Aug. 2017, ISBN: 956975g4516.
- [34] M. Hall, "MoorDyn V2: New Capabilities in Mooring System Components and Load Cases: Preprint," in *ASME 2020 39th International Conference on Ocean, Offshore and Arctic Engineering*, National Renewable Energy Laboratory, Golden, CO, Sep. 2020. [Online]. Available: www.nrel.gov/publications.
- [35] A. Pegalajar-Jurado, M. Borg, and H. Bredmose, "An efficient frequency-domain model for quick load analysis of floating offshore wind turbines," *Wind Energy Science*, vol. 3, no. 2, pp. 693–712, 2018, ISSN: 23667451. DOI: 10.5194/wes-3-693-2018.
- [36] A. Pegalajar-Jurado, H. Bredmose, M. Borg, *et al.*, "State-of-the-art model for the LIFES50+ OO-Star Wind Floater Semi 10MW floating wind turbine," in *Journal of Physics: Conference Series*, vol. 1104, Institute of Physics Publishing, Nov. 2018. DOI: 10.1088/1742-6596/1104/1/012024.
- [37] F. J. Madsen, A. Pegalajar-Jurado, and H. Bredmose, "Performance study of the QuLAF pre-design model for a 10MW floating wind turbine," *Wind Energy Science*, vol. 4, no. 3, pp. 527–547, Sep. 2019, ISSN: 23667451. DOI: 10.5194/wes-4-527-2019.
- [38] N. Pollini, A. Pegalajar-Jurado, S. Dou, H. Bredmose, and M. Stolpe, "Gradient-based optimization of a 15 MW wind turbine spar floater," in *Journal of Physics: Conference Series*, vol. 2018, IOP Publishing Ltd, Sep. 2021. DOI: 10.1088/1742-6596/2018/1/012032.
- [39] S. Dou, A. Pegalajar-Jurado, S. Wang, H. Bredmose, and M. Stolpe, "Optimization of floating wind turbine support structures using frequency-domain analysis and analytical gradients," in *Journal of Physics: Conference Series*, vol. 1618, IOP Publishing Ltd, Sep. 2020. DOI: 10.1088/1742-6596/1618/4/042028.
- [40] M. K. Al-Solihat and M. Nahon, "Stiffness of slack and taut moorings," *Ships and Offshore Structures*, vol. 11, no. 8, pp. 890–904, Nov. 2016, ISSN: 17445302. DOI: 10.1080/17445302.2015.1089052.
- [41] M. Hall, S. Housner, D. Zalkind, P. Bortolotti, D. Ogden, and G. Barter, "An Open-Source Frequency-Domain Model for Floating Wind Turbine Design Optimization," in *Journal of Physics: Conference Series*, vol. 2265, Institute of Physics, Jun. 2022. DOI: 10.1088/1742-6596/2265/4/042020.
- [42] M. Hall, S. Housner, S. Srinivas, and S. Wilson, *MoorPy*, Golden, CO, Jul. 2021.
- [43] A. C. Pillai, P. R. Thies, and L. Johannig, "Mooring system design optimization using a surrogate assisted multi-objective genetic algorithm," English, *Engineering Optimization*, vol. 51, no. 8, pp. 1370–1392, 2019, ISSN: 0305215X (ISSN). DOI: 10.1080/0305215X.2018.1519559. [Online]. Available: <https://www.scopus.com/inward/record.uri?eid=2-s2.0-85055278612&doi=10.1080%2f0305215X.2018.1519559&partnerID=40&md5=bbd93c9b47b74b9043474569c1b03043>.
- [44] K. Deb and H. Jain, "An evolutionary many-objective optimization algorithm using reference-point-based nondominated sorting approach, Part I: Solving problems with box constraints," *IEEE Transactions on Evolutionary Computation*, vol. 18, no. 4, pp. 577–601, 2014, ISSN: 1089778X. DOI: 10.1109/TEVC.2013.2281535.
- [45] W. West, A. Goupee, S. Hallowell, and A. Viselli, "Development of a Multi-Objective Optimization Tool for Screening Designs of Taut Synthetic Mooring Systems to Minimize Mooring Component Cost and Footprint," *Modelling*, vol. 2, no. 4, pp. 728–752, Dec. 2021, ISSN: 26733951. DOI: 10.3390/modelling2040039.
- [46] W. M. West, A. J. Goupee, S. T. Hallowell, and A. M. Viselli, "Determination of minimum-cost synthetic mooring systems for large floating wind turbines deployed in intermediate water depths," English, *Journal of Renewable and Sustainable Energy*, vol. 15, no. 1, 2023, ISSN: 19417012 (ISSN). DOI: 10.1063/5.0123474. [Online]. Available: <https://www.scopus.com/inward/record.uri?eid=2-s2.0-85148477303&doi=10.1063%2f5.0123474&partnerID=40&md5=2c043a1e80d1b368d6680142541b569c>.
- [47] P. T. Boggs and J. W. Tolle, "Sequential Quadratic Programming," *Acta Numerica*, pp. 1–52, 1996.
- [48] C. J. A. Janus, "Layout Optimisation of Floating Offshore Wind Farms Minimisation of inter-array cable length while allowing for anchor-sharing in a floating offshore wind farm," Ph.D. dissertation, Delft University of Technology, Delft, NL, Jan. 2024.

- [49] M Karimi, M Hall, B Buckham, and C Crawford, "A multi-objective design optimization approach for floating offshore wind turbine support structures," English, *Journal of Ocean Engineering and Marine Energy*, vol. 3, no. 1, pp. 69–87, 2017, ISSN: 21986444 (ISSN). DOI: 10.1007/s40722-016-0072-4. [Online]. Available: <https://www.scopus.com/inward/record.uri?eid=2-s2.0-85019162638&doi=10.1007%2fs40722-016-0072-4&partnerID=40&md5=32bf35ce6cb484259c10999e9472929f>.
- [50] "Olie-og naturgasindustri-Specifikke krav til offshorekonstruktioner-Del 4: Geotekniske og funderingsmaessige beregningshensyn Petroleum and natural gas industries-Specific requirements for offshore structures-Part 4: Geotechnical and foundation design considerations," Tech. Rep., 2016.
- [51] E. Wayman, "Coupled Dynamics and Economic Analysis of Floating Wind Turbine Systems," Tech. Rep., 2004.
- [52] M Hall, B Buckham, and C Crawford, "Evolving offshore wind: A genetic algorithm-based support structure optimization framework for floating wind turbines," English, in *OCEANS 2013 MTS/IEEE Bergen: The Challenges of the Northern Dimension*, 2013, ISBN: 978-147990001-5 (ISBN). DOI: 10.1109/OCEANS-Bergen.2013.6608173. [Online]. Available: <https://www.scopus.com/inward/record.uri?eid=2-s2.0-84886403487&doi=10.1109%2fOCEANS-Bergen.2013.6608173&partnerID=40&md5=96990e715da643b09bac336fffd24b79>.
- [53] K. Deb, A. Pratap, S. Agarwal, and T. Meyarivan, "A Fast and Elitist Multiobjective Genetic Algorithm: NSGA-II," Tech. Rep. 2, 2002.
- [54] D. Cazzaro and D. Pisinger, "Synthetic Instances for Large Offshore Wind Farm Layout," Technical University of Denmark, Lyngby, DK, Tech. Rep., Nov. 2021.
- [55] "Metocean Study Ten noorden van de Waddeneilanden Wind Farm Zone," Netherlands Enterprise Agency, Tech. Rep., May 2022.
- [56] "RECOMMENDED PRACTICE Fatigue design of offshore steel structures," Tech. Rep., 2019.
- [57] DNV AS, "DNV-ST-0119 Floating wind turbine structures," Tech. Rep., 2021.